NASA TECHNICAL NOTE

NASA TN D-4600



NASA TN D-4600



# ANALYSIS AND SELECTION OF DESIGN CONDITIONS FOR A RADIOISOTOPE BRAYTON-CYCLE SPACE POWERPLANT

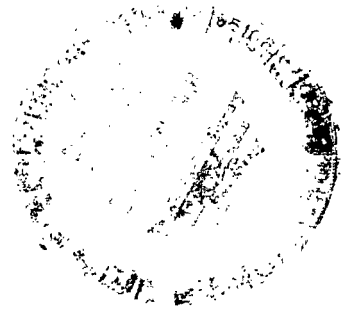

*by John L. Klann*

*Lewis Research Center*
*Cleveland, Ohio*

NATIONAL AERONAUTICS AND SPACE ADMINISTRATION • WASHINGTON, D. C. • JUNE 1968

NASA TN D-4600

# ANALYSIS AND SELECTION OF DESIGN CONDITIONS FOR A RADIOISOTOPE BRAYTON-CYCLE SPACE POWERPLANT

By John L. Klann

## APPENDIX D: HEAT SOURCE ANALYSIS

By John L. Klann, Leonard Soffer, and Gerald J. Barna

## APPENDIX E: HEAT-EXCHANGER ANALYSIS

By John L. Klann, Gabriel N. Kaykaty, Paul T. Kerwin, and Darl D. Bien

Lewis Research Center
Cleveland, Ohio

NATIONAL AERONAUTICS AND SPACE ADMINISTRATION

For sale by the Clearinghouse for Federal Scientific and Technical Information
Springfield, Virginia 22151 – CFSTI price $3.00

## ABSTRACT

Selections were made for a conceptual plutonium 238 module for electric powers in the range from 2 to 10 kilowatts. Based on the selections, component and system efficiency and weight were estimated for powers of 2, 6, and 10 kilowatts.

STAR Category 03

# CONTENTS

# ANALYSIS AND SELECTION OF DESIGN CONDITIONS FOR A RADIOISOTOPE BRAYTON-CYCLE SPACE POWERPLANT

by John L. Klann

Lewis Research Center

## SUMMARY

A parametric analysis of a conceptual plutonium 238 radioisotope Brayton-cycle space powerplant was conducted. Major design variables were investigated to define design conditions which result in relatively compact and efficient power modules for electric powers in the range from 2 to 10 kilowatts.

For the powerplant concept, a plane array of radioisotope capsules with a maximum capsule-wall temperature of 2460° R (1367° K) radiated its heat to the adjacent heat exchanger of the power conversion unit. In the power conversion unit, a mixture of helium and xenon drove a single combined rotating unit consisting of a single-stage, radial-flow compressor and turbine and a brushless generator of the Lundell type, all supported by gas bearings. Waste cycle heat was rejected by a separate liquid-filled coolant loop.

As a result of this analysis, the major Brayton cycle parameter selections were: turbine inlet temperature, 2060° R (1144° K); compressor inlet temperature, 540° R (300° K); working fluid molecular weight, 83.8; shaft speed, 36 000 rpm (3770 rad/sec); compressor pressure ratio, 1.90; compressor specific speed, 0.775; system loss pressure ratio, 0.92; and recuperator effectiveness, 0.95. Based on these selections, overall system efficiency (the ratio of net electrical power to initial isotope thermal power), unshielded system specific weights, and shielded specific weights were estimated as follows:

| Net power, kW | Overall efficiency | Unshielded specific weight | | Shielded specific weight | |
|---|---|---|---|---|---|
| | | lb/kWe | kg/kWe | lb/kWe | kg/kWe |
| 2 | 0.18 | 990 | 449 | 1590 | 724 |
| 6 | .23 | 490 | 222 | 850 | 386 |
| 10 | .24 | 440 | 200 | 740 | 336 |

# INTRODUCTION

Lewis Research Center is currently engaged in a program for advancing closed Brayton cycle technology with its ultimate intent of generating electric power in space. The initial efforts were centered about a solar-powered concept which is described in reference 1. The power conversion unit of that concept was designed to supply 8 kilowatts of electric power at 400 hertz. It was characterized by two separate, main rotating units, namely, a turbine-driven compressor (turbocompressor) and a power-producing turboalternator. Some components for this concept are presently being tested. Although initially based on the solar-powered concept, the power conversion unit may also be employed with other energy sources.

Reference 2 shows that radioisotopes are a promising heat source for a Brayton-cycle conversion unit. Successful development of safe, multikilowatt radioisotope heat sources coupled with Brayton-cycle power conversion modules would offer additional spacecraft flexibility. Reference 3, for example, demonstrates the applicability of such a power system to a conceptual manned orbiting research laboratory. Two operative 5.5-kilowatt (net electric) modules, each with an additional power conversion unit on standby, are used to enhance system reliability and maintenance. In comparison with solar-powered systems, the radioisotope-fueled systems do not require either orientation toward the Sun or large extended sunlight-collecting surfaces.

The analysis presented herein was conducted to define desirable design conditions for an isotope-fueled power conversion module. Because of the limited availability of the more desirable radioisotopes (ref. 2), the basic goal was high overall system conversion efficiency. This goal was to be accomplished wherever possible with minimum weight but without excessive penalty to system volume.

The analysis was restricted to a consideration of a single combined rotating unit - turbine, alternator, and compressor - supported by gas bearings and on a common shaft. The power range from 2 to 10 kilowatts was chosen for investigation. Although any given power system must have the capability of producing power on demand from zero to a nominal, rated value, the rated power output itself might also be adjusted for each given application. For a given Brayton combined rotating unit, this would be done by selecting a gas pressure level at, for instance, the compressor inlet. Hence, as part of this analysis, the feasibility of using one combined rotating unit over the range of rated power output from 2 to 10 kilowatts was also investigated.

Gross shielding approximations and factors affecting fuel-block geometry and weight are presented in appendix D by John L. Klann, Leonard Soffer, and Gerald J. Barna. Brief descriptions of the calculations and typical results for each of the cycle heat-transfer components are presented in appendix E by John L. Klann, Gabriel N. Kaykaty, Paul T. Kerwin, and Darl D. Bien.

# METHOD OF ANALYSIS

In order to facilitate the analysis, a conceptual power system was hypothesized, and a reference set of conditions was established. Because of the large number of parameters, each major variable was varied individually while the others were kept at the initial reference conditions. Thermodynamic variations were investigated first to determine trends and desirable ranges of conditions for further analysis. Then, component- and system weight and volume variations were investigated. Based on this analysis of first-order variations, a set of preliminary operating conditions was selected. These conditions were then applied to the conceptual powerplant at 2-, 6-, and 10-kilowatt power levels, and overall system performance was evaluated.

## Conceptual Power System

A schematic diagram of the assumed power conversion unit is shown in figure 1. Cycle state-point numbering is shown in figure 1. (All symbols are defined in appendix A.) The three major subsystems are a radioisotope heat source, a gas-filled power-conversion loop, and a liquid-filled heat-rejection loop. Radiation heat transfer between the heat source and the heat-source heat exchanger was assumed. The Brayton-cycle

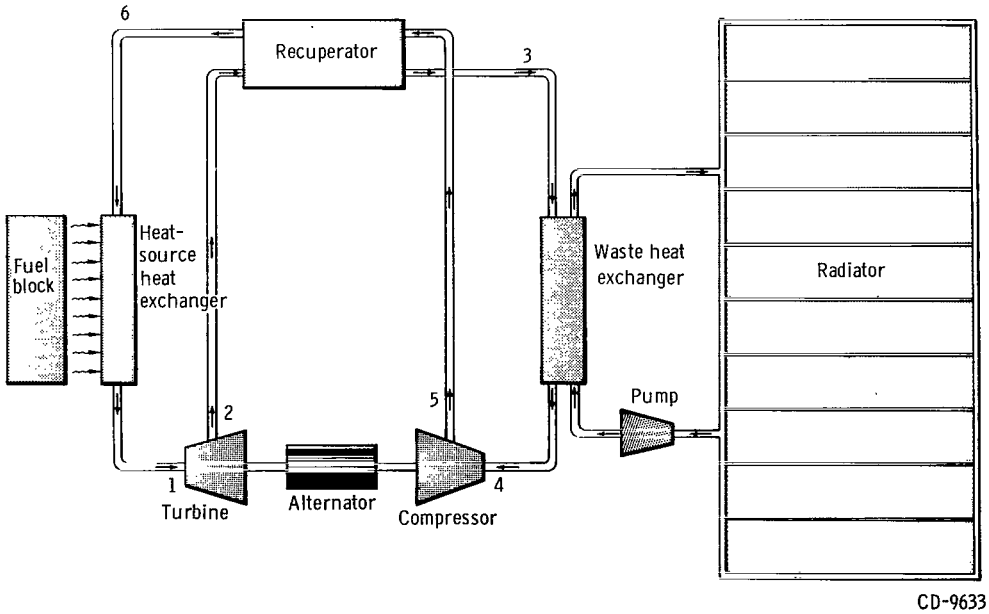


Figure 1. - Schematic diagram of powerplant.

working fluid was assumed to be a mixture of helium and xenon (refs. 4 and 5). Recuperation was assumed. Both the compressor and turbine of the single-shaft combined rotating unit were assumed to be single-stage radial-flow machines, while the alternator was a brushless generator of the Lundell type. The combined rotating unit was assumed to be supported hydrodynamically by bearings using the prime working gas. Cycle waste energy was assumed to be rejected by the secondary, liquid-filled coolant loop. This required a gas-to-liquid waste heat exchanger, a radiator, and a pump. The pump was assumed to be motor driven and separate from the prime turbomachinery.

## Thermodynamic Calculations

Single-stage radial-flow turbine and compressor efficiency models were hypothesized and empirically fitted to experimental results obtained from component testing (ref. 6). Efficiency was assumed to be a function of specific speed, specific diameter, Reynolds number, characteristic tip Mach number, and tip diameter. These models (presented in appendix B) were included in the basic cycle thermodynamic calculation procedure (presented in appendix C). Hence, effects of machinery size, speed, and pressure level on cycle thermal efficiency (the ratio of gross shaft power to cycle thermal input power $P_{sh}/Q_{in}$) were evaluated.

Table I shows the initial reference conditions and the range of parameters investigated for basic cycle performance. The helium-xenon gas mixture (used because of its increased heat-transfer capability in comparison with pure gases) was investigated for the average molecular weights of krypton (83.8) and also, but less thoroughly, of argon (39.9). Although the use of a gas mixture is advantageous, the ability to maintain the proper molecular weight remains to be demonstrated. Limiting the analysis and design considerations to the molecular weights of krypton and argon, rather than to a range of molecular weights, would permit substitution of the single gas without an appreciable effect on rotating component efficiency. Such a substitution, however, would result in reduced overall conversion efficiency because of reduced heat transfer.

Turbine inlet temperatures investigated were $1860^{\circ}$, $1960^{\circ}$, and $2060^{\circ}$ R ($1033^{\circ}$, $1089^{\circ}$, and $1144^{\circ}$ K). A basic guideline for the analysis was to use nonrefractory metals for all components except the heat source. The selected range of turbine inlet temperature was presumed to be permissible for long-term use of nonrefractory alloys.

At each turbine inlet temperature, compressor inlet temperature was varied over a range bounded by $490^{\circ}$ and $720^{\circ}$ R ($272^{\circ}$ and $400^{\circ}$ K). The other major variables included recuperator effectiveness, system loss pressure ratio (i.e., that portion of the compressor pressure ratio which is available to the turbine), compressor pressure ratio, shaft

TABLE I. - INITIAL REFERENCE CONDITIONS AND RANGE OF PARAMETERS FOR THERMODYNAMIC CALCULATIONS

| Parameter | Initial reference condition | Range or other conditions |
|---|---|---|
| Working fluid | Helium-xenon | ---------- |
| Molecular weight, $M_w$ | 83.8 | 39.94 |
| Turbine inlet temperature, $T_1$: | | |
| $^oR$ | 1960 | 1860, 2060 |
| $^oK$ | 1089 | 1033, 1144 |
| Compressor inlet temperature, $T_4$: | | |
| $^oR$ | 540 | 490 to 720 |
| $^oK$ | 300 | 272 to 400 |
| Recuperator effectiveness, $E_r$ | 0.900 | 0.875 to 0.950 |
| Loss pressure ratio, L | 0.900 | 0.900 to 0.950 |
| Compressor pressure ratio, $p_5/p_4$ | 1.90 | 1.60 to 3.60 |
| Rotational speed, N: | | |
| rpm | 36 000 | 24 000; 48 000; 60 000 |
| rad/sec | 3770 | 2510; 5020; 6280 |
| Compressor specific speed, $N_{s,c}$ | 0.775 | 0.54 to 0.86 |
| Turbine-exit-loss parameter, $L_e$ | 0.04 | ---------- |
| Equivalent sink temperature, $T_s$: | | |
| $^oR$ | 450 | ---------- |
| $^oK$ | 250 | ---------- |
| Radiator surface emittance, $\epsilon$ | 0.90 | ---------- |
| Pressure-drop distribution ratio, $\alpha$ | 0.50 | ---------- |
| Compressor slip factor, $\beta$ | 0.85 | ---------- |
| Turbine blade-jet speed ratio, $\nu$ | 0.70 | ---------- |
| Waste-heat-exchanger effectiveness, $E_s$ | 0.95 | ---------- |
| Waste-heat-exchanger capacity rate ratio, $C_s$ | 0.87 | ---------- |

rotational speed, and compressor specific speed. The rotational speeds investigated were chosen to yield multiples of 400-hertz output frequencies for four-pole alternators.

The remaining parameters (listed in table I) were assigned reasonable values but were not varied. The turbine-exit-loss parameter, defined as the square of the ratio of the axial component of the velocity to the ideal jet speed, was set at 0.04. Reference 7 shows this to be a lower limit for stable flow conditions in radial inflow turbines. This loss parameter is a measure of the turbine-exit kinetic energy and relates total to static

efficiency (eq. (C24)). Turbine static efficiency has been used in this analysis, and hence the exit kinetic energy, although made small, was assumed to be lost to the system. The assumed equivalent sink temperature is a few degrees below the maximum equivalent sink temperature for an unoriented, cylindrical radiator in a low Earth orbit. The assumed radiator surface emittance is within the state of the art for low-temperature surfaces. The pressure-drop distribution ratio is the ratio of fractional pressure drop $\Delta p/p$ on the high-pressure side of the cycle to that on the low-pressure side. The compressor slip factor and the turbine blade to jet speed were taken as representative values for efficient designs.

## Weight Calculations

Results of the thermodynamic calculations were used as input conditions for the determination of size and weight tradeoffs among the components. The same approach used in the thermodynamic calculations was used for the weight calculations. Each major variable was investigated individually while the others were kept at the initial reference conditions. The variables were turbine inlet temperature, compressor inlet temperature, recuperator effectiveness, system loss pressure ratio, and to a limited extent, working fluid and its molecular weight. Shaft power level was set at 6.875 kilowatts as representative of the midrange of net system output.

In addition, particular geometries were assumed for each component. A manned 5-year mission was postulated for sizing the heat source and radiator. As in reference 2, the heat source was assumed to be a flat slab (referred to as "fuel block") formed by a matrix of closely packed fuel capsules joined together by a niobium web. The fuel was assumed to be plutonium 238 in a dioxide form. The fuel block was sized to be capable of rejecting its initial heat production without normally exceeding a temperature of $2460^{\circ}$ R ($1367^{\circ}$ K). The initial inventory allowed for isotope decay over the assumed 5-year mission and an assumed 90-day launch delay. Single-sided thermal radiation from one face of the fuel block to the heat-source heat exchanger was assumed.

Figure 2 depicts the assumed installation of the power system in a mission vehicle. The power system was assumed to be placed near the cylindrical wall at the aft end of a 260-inch- (6.6-m-) diameter manned vehicle. The radiator was assumed to encompass this portion of the vehicle. Immediately inside the thermally insulated door is the radioisotope heat source mounted on a reentry body. Nuclear shielding was assumed to enclose the fuel block and heat-source heat exchanger on all sides excepting those which face away from the manned compartment. Thermal insulation might be required on the inside of the shield in order to keep the shielding material at reasonable temperatures.

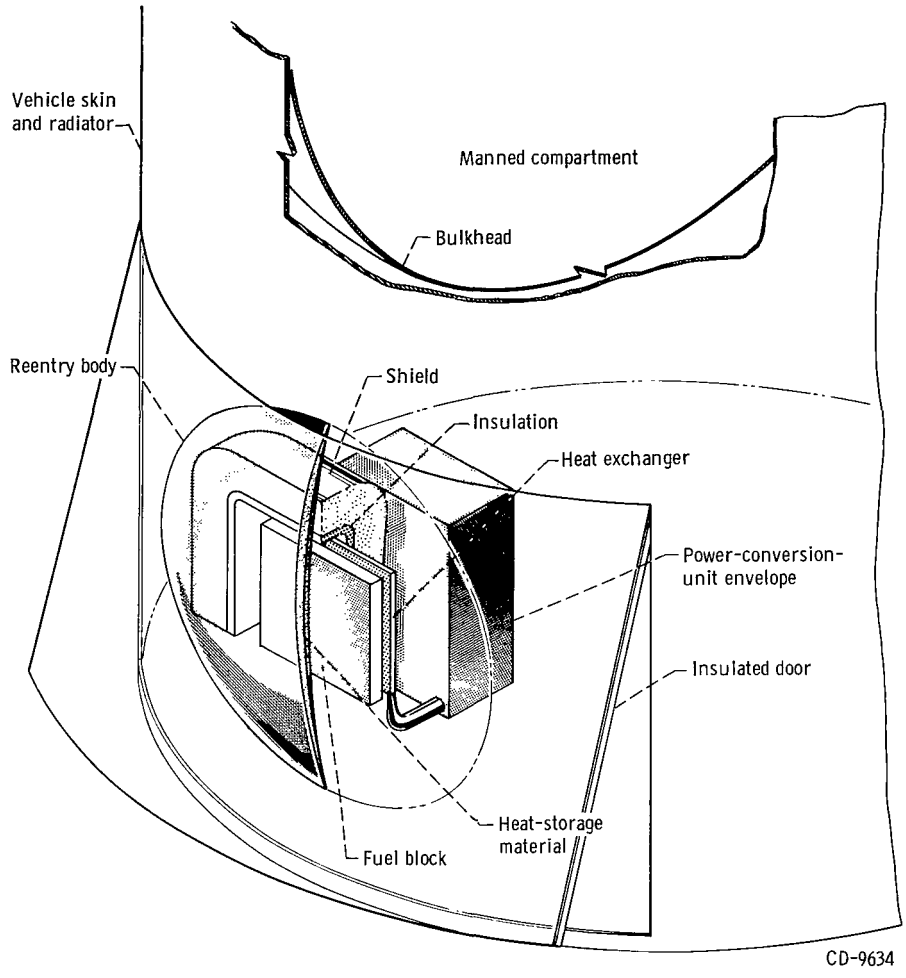


Figure 2. - Conceptual powerplant installation.

The hot gas mixture is ducted from the heat-source heat exchanger around the shield to the power conversion unit.

Analysis of the fuel block and gross approximation of the shield thickness and weight are presented in appendix D. For the general analysis of fuel block size and weight, one layer of fuel capsules was assumed. Each capsule had a void volume to allow for a maximum internal helium pressure of 10 000 psi (69 $MN/m^2$) (see ref. 2 for details). Capsule burial criteria were not considered. Shield weights were calculated for constant nuclear dose rates of 1 and 5 millirems per hour at a distance of 10 feet (3 m) from the source. These dose rates were considered to be representative of conservative and liberal allowances, respectively, for a manned spacecraft.

Details of the four heat-exchanger analyses are presented in appendix E. The heat-source heat exchanger was assumed to have a once-through plate-fin arrangement, while

the recuperator employed a rectangular offset-fin counterflow core with triangular end sections. The heat-sink heat exchanger was assumed to have a multipass cross counterflow tube-fin arrangement. This exchanger was sized to fit directly on the appropriate recuperator end section. A cylindrical, unoriented radiator with longitudinal finned tubes and circumferential headers on the 260-inch- (6.6-m) diameter vehicle was assumed. Two complete coolant circuits (one redundant) sharing common fins were so armored against meteroid penetration that the probability of survival of at least one coolant circuit at the end of 5 years was 0.995. The fluorocarbon FC-75 (ref. 8, p. 86) was selected as the radiator coolant.

## System Efficiency

In the evaluation of overall system efficiency, calculations or allowances were made for some of the thermal, mechanical, and electrical losses. Details are presented in appendix F. Allowances were made for heat-source thermal loss, system control power, and liquid-coolant-loop pump power. Estimates were made for bearing friction loss, alternator electromagnetic and windage losses, and shaft seal loss for the combined rotating unit. No direct allowance was made for thermal loss through the insulation surrounding the conversion loop. Although it was assumed that the combined rotating unit alternator and the control system electronics would be cooled by the radiator coolant, these heat loads were not included in the radiator calculations. These heat loads might add 15 to 25 percent to the rejected heat for power outputs of 10 to 2 kilowatts, respectively, but because these heat loads do not change rapidly with the design variables in table I, their inclusion in or omission from the analysis has only a minor effect on selection of desirable design conditions for the power system.

"System efficiency" is herein defined as the ratio of alternator output power less pump and control power to the gross initial thermal energy from the isotope package. Gross initial isotope energy allowed for decay over the mission life, heat-source thermal loss, and required cycle thermal input, and no credit for the initial excess thermal energy available from the heat source was taken.

## System Variations with Power Level

Design parameters from this first-order thermodynamic and weight analysis were used to define the conceptual powerplant. Its efficiency and total weight were estimated for net output power levels of 2, 6, and 10 kilowatts. The combined rotating unit was sized for operation over the entire power range, while all other components were resized

at each power level. Hence, the selected values for turbine inlet temperature, compressor inlet temperature, recuperator effectiveness, and system loss pressure ratio were maintained at each power level. Although the system loss pressure ratio was fixed, the individual conversion-loop-component pressure drops were redistributed at each power level in order to yield minimum combined heat-exchanger weight (appendix E).

Total system weight estimates are based on the power system arrangement in figure 2. The heat-source subsystem weight estimates include the fuel block, reentry body, and a quantity of emergency heat-storage material. This combined heat-source package is configured to contain the radioisotope fuel safely under a variety of conditions. Details of the concept are presented in reference 2 and further explored in references 9 and 10. The reentry body permits separate intact return of the isotope capsules from orbit, while the main purpose of the heat-storage material is to prevent capsule melting and isotope release as the result of a launch-pad explosion and fire and subsequent entrapment of the heat source beneath the burned out wreckage of the launch vehicle. In the present analysis, enough heat-storage material was assumed (based on the work of ref. 10) for approximately a 90-minute delay in recovery of the heat source after such an accident.

On the basis of minimum combined fuel-block and shield weight, the fuel block was assumed to have one layer of capsules with each capsule void volume sized for a maximum internal pressure of 12 500 psi (86.1 $MN/m^2$) rather than the 10 000 psi (69 $MN/m^2$) assumed in Weight Calculations which resulted in somewhat higher weight (appendix D). Both the reentry body and heat-storage weights were estimated from the results of references 9 and 10. The reentry body was assumed to be approximately 20 percent of the total heat-source weight, while the heat-storage material was assumed to be beryllium oxide estimated from references 9 and 10 as 150 pounds (68 kg) for a 25-kilowatt-thermal source.

The heat-exchanger weights were estimated from the analysis in appendix E. The weight of the combined rotating unit was based on a detailed design. Ducting, structure, and control system weights were scaled from the results of reference 3. A specific radiator area of 90 square feet per kilowatt electric (8.36 $m^2/kWe$) was assumed so that radiator weight near the minimum could be achieved at each power level. Structural aspects of the radiators were not considered. The shield weight estimates were based on a dose rate of 5 millirems per hour at a distance of 10 feet (3 m) from the isotope heat source.

## RESULTS AND DISCUSSION

First-order variations of major power-conversion-unit parameters are presented in the sections Thermodynamic Variations and Weight Variations. The final section Selections and Performance Estimates summarizes the results.

## Thermodynamic Variations

A performance map for the initial reference conditions of table I is shown in figure 3. Cycle thermal efficiency (the ratio of gross shaft power to required cycle thermal input, where gross shaft power is the turbine power minus compressor power) is plotted against specific prime radiator area (the ratio of prime or minimum radiator area[1] to gross shaft power) with compressor pressure ratio and inlet temperature as independent parameters. For a fixed compressor pressure ratio, cycle efficiency approaches a maximum as the compressor inlet temperature approaches the sink temperature (450° R, or 250° K). At this condition, the largest cycle temperature difference, and hence efficiency, is available; however, the radiator area becomes large. For a fixed value of compressor inlet temperature, cycle efficiency exhibits a maximum with respect to

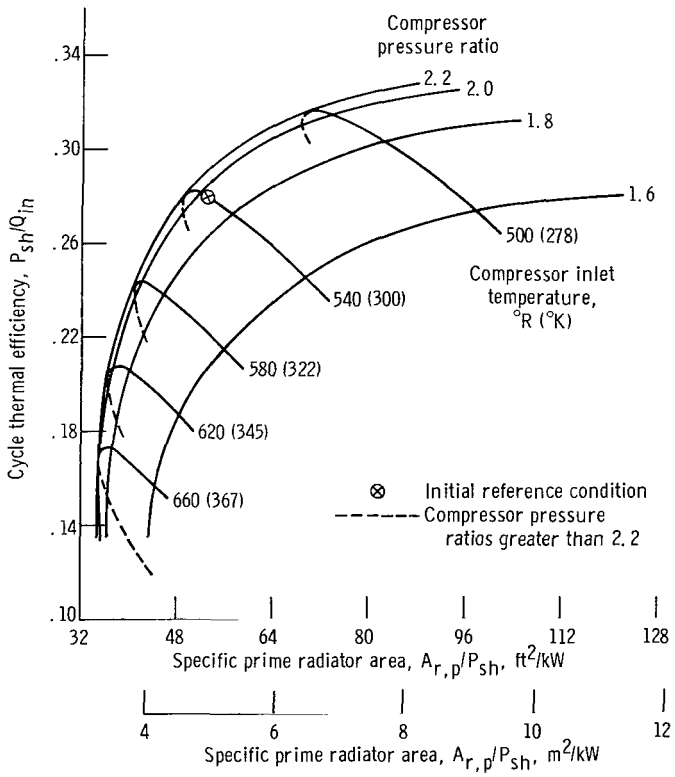


Figure 3. - Brayton cycle performance. (All other initial reference conditions of table I apply.)

[1]In the thermodynamic calculations, prime or minimum radiator area is approximated by neglecting the drop between the bulk liquid temperature and the radiating surface temperature (eq. (C36)).

compressor pressure ratio. The variations in specific prime radiator area with compressor inlet temperature and pressure ratio result from combined effects of radiator heat load and average radiator temperature level.

The general level of performance shown in figure 3 is dependent not only on the assigned cycle conditions, but also on the calculated turbine and compressor efficiencies (appendix B). The ranges of efficiency calculated for this figure were 0.847 to 0.855 and 0.754 to 0.771 for the turbines and compressors, respectively. Since these variations were relatively small, the general shape of these curves is similar to that reported in other analyses using fixed turbine and compressor efficiencies (ref. 11, e.g.).

Turbine- and compressor-inlet temperatures. - Figure 4 shows the variation of cycle thermal efficiency and specific prime radiator area with compressor inlet temperature for three turbine inlet temperatures. Compressor inlet temperature is shown only for the range of interest, namely, $500^{\circ}$ to $630^{\circ}$ R ($278^{\circ}$ to $350^{\circ}$ K), where the high value is close to that for minimum specific prime radiator area. At the reference value of compressor inlet temperature ($540^{\circ}$ R, or $300^{\circ}$ K), cycle efficiency increased by approximately 0.02 (or about 8 percent) for each $100^{\circ}$ R ($56^{\circ}$ K) increase in turbine

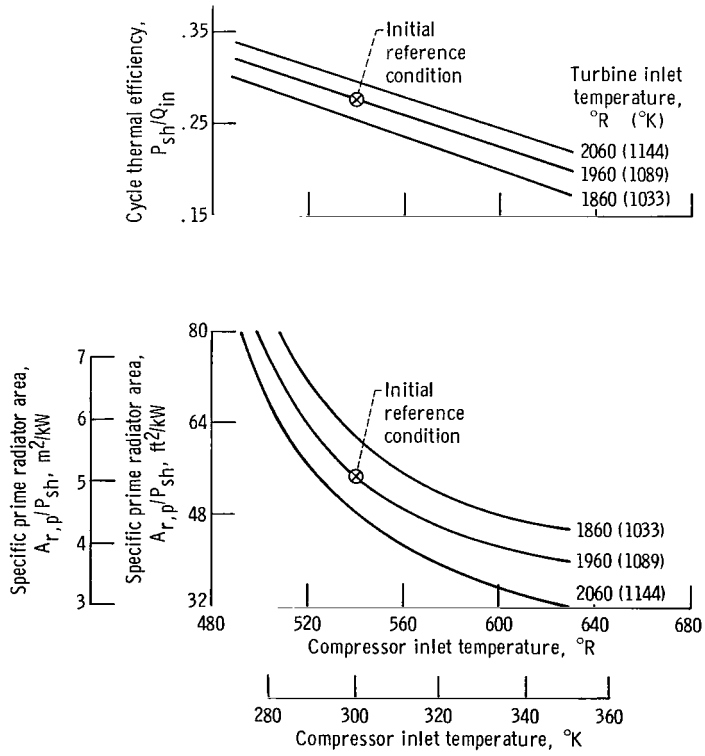


Figure 4. - Effect of compressor- and turbine-inlet temperature on specific prime radiator area and cycle thermal efficiency. (All other initial reference conditions of table I apply.)

inlet temperature above 1860° R (1033° K), but specific prime radiator area decreased by approximately 6.5 square foot per kilowatt or 0.6 square meter per kilowatt (or about 10 percent) for the same changes. For this example, predicted turbine and compressor efficiencies decreased from 0.850 and 0.765 to 0.847 and 0.763, respectively, between 1860° and 2060° R (1033° and 1144° K).

On the basis of cycle performance alone, the highest tolerable turbine inlet temperature should be chosen.

Compressor specific speed. - Variations in turbine- and compressor-efficiency, size, and pressure level due to changes in compressor specific speed are a direct result of the assumed turbomachinery efficiency models (see appendix B). Variation in cycle efficiency and specific prime radiator area with compressor pressure ratio and specific speed is shown in figure 5(a). As compressor specific speed increases from 0.5425 to 0.7750 for any value of compressor pressure ratio, cycle efficiency increases, and specific prime radiator area decreases. Near-maximum cycle efficiencies are obtained for compressor specific speeds from 0.6975 to 0.7750. Increasing compressor specific speed from 0.7750 to 0.8525 reduces cycle efficiency. Maximum cycle efficiency occurs at a compressor pressure ratio of about 2.1 for any compressor specific speed.

Maximum system efficiency tends to occur at slightly lower values of compressor pressure ratio than those which result in maximum cycle efficiency. Among the parasitic losses included in the calculation of system efficiency, alternator windage decreases and bearing and seal losses increase with increasing compressor pressure ratio, whereas the others remain essentially constant (see appendix F for details).

Figure 5(b) shows the effect of compressor specific speed on turbine and compressor efficiencies, the specific compressor inlet pressure (the ratio of compressor inlet pressure to gross shaft power), and the required tip diameters, all over a range of compressor pressure ratio from 1.5 to 2.8. Decreasing compressor pressure ratio increases the specific compressor inlet pressure and decreases turbine and compressor diameters. At the same time, compressor efficiency improves (mainly because of the beneficial effect of pressure ratio; see appendix B) and turbine efficiency remains essentially unchanged (because of conflicting effects of size, pressure ratio, and Reynolds number; see appendix B). For any compressor pressure ratio, decreasing compressor specific speed increases the specific compressor inlet pressure, slightly increases compressor tip diameter, and decreases compressor efficiency. Turbine efficiency, however, first increases and then decreases with decreasing compressor specific speed, when the compressor pressure ratio is fixed.

One reason for selecting a compressor specific speed below 0.775 might be to increase overall system pressure level. For example, at the reference pressure ratio (1.90), reductions of compressor specific speed from 0.7750 to 0.6975, 0.6200, and 0.5425 increased compressor inlet pressure (for a fixed shaft power) by about 23, 62,

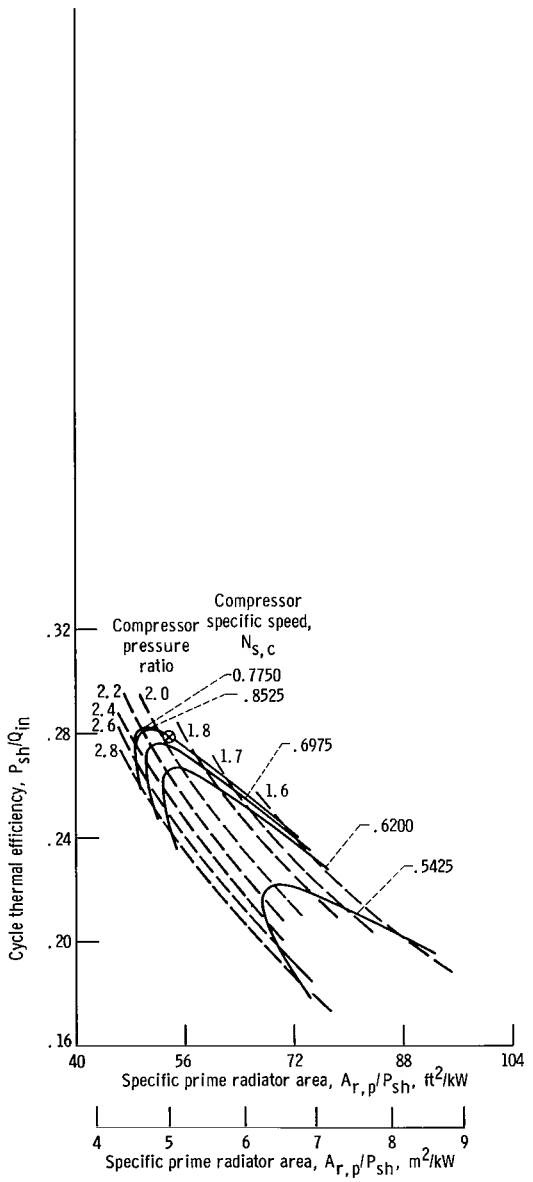


(a) Specific prime radiator area and cycle thermal efficiency variations.

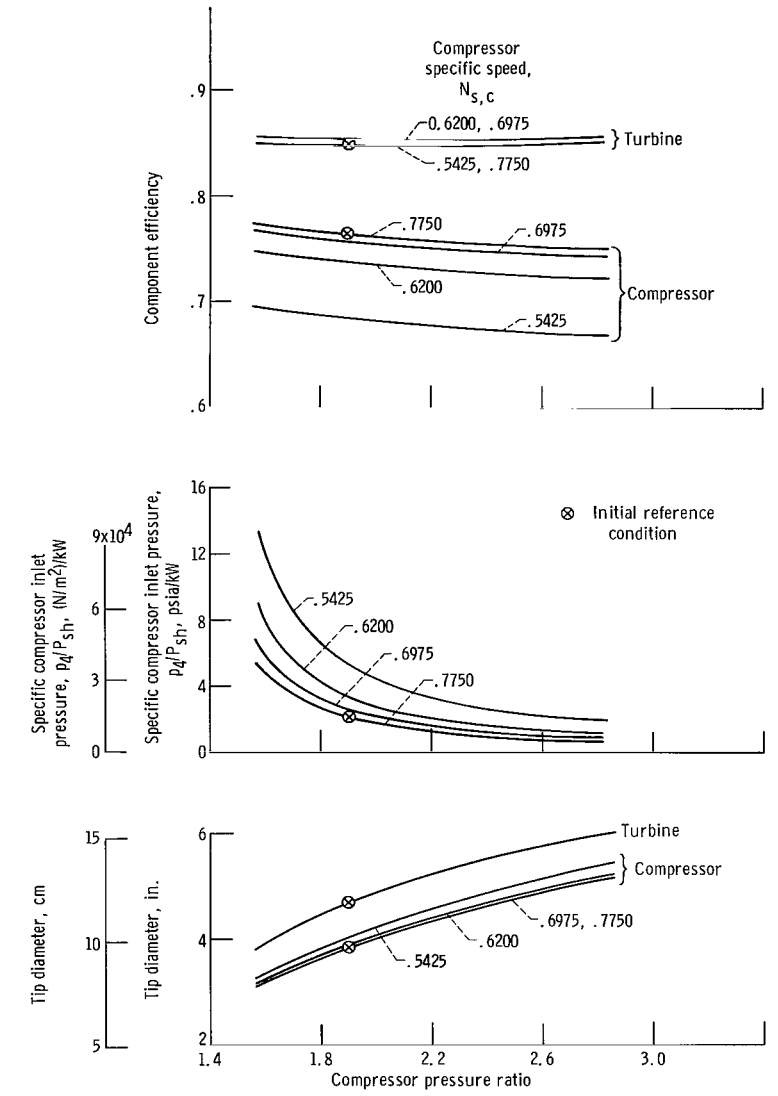


(b) Pressure level and turbomachinery variations.

Figure 5. - Effect of compressor specific speed on performance. (All other initial reference conditions of table I apply.)

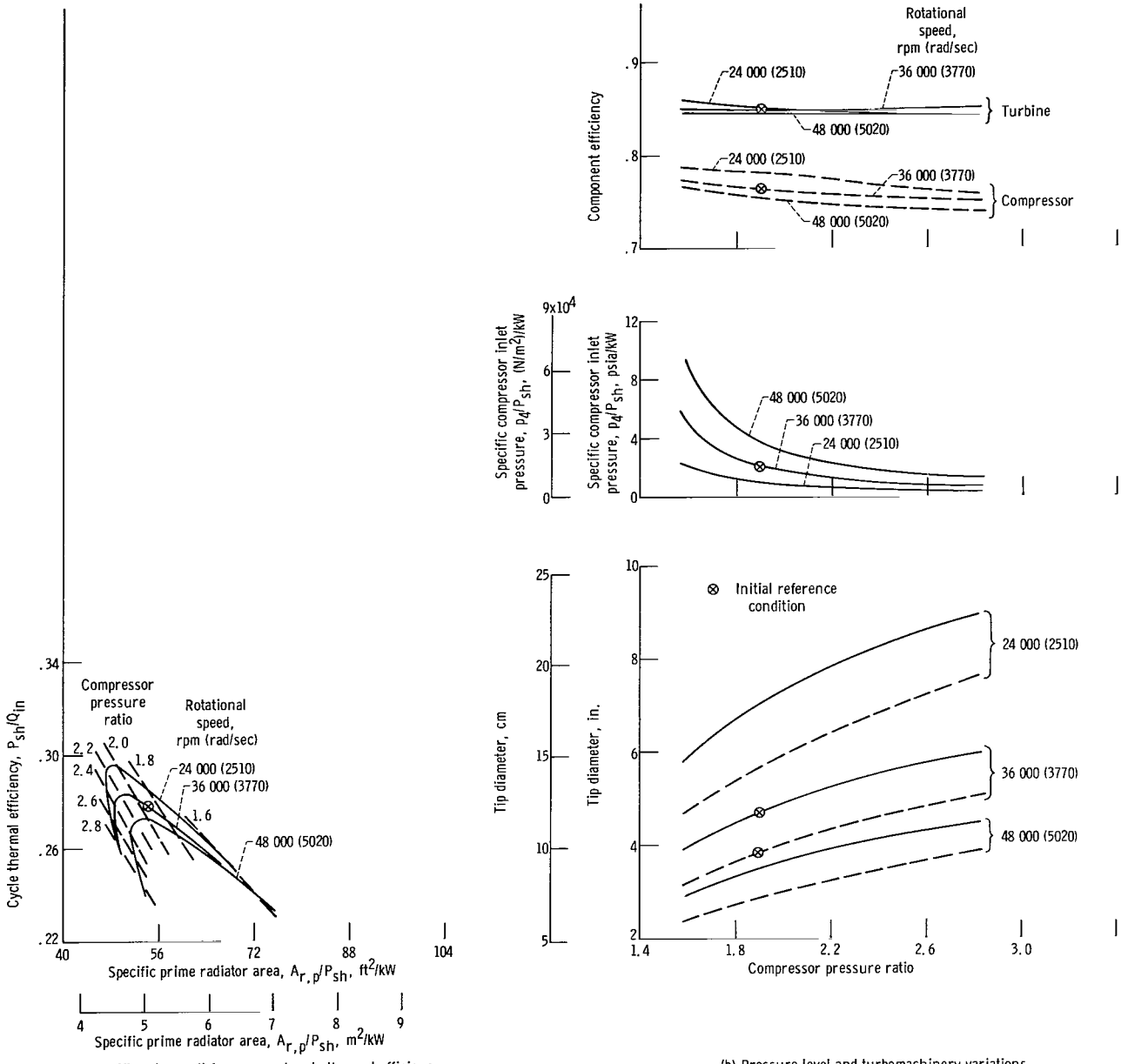


(a) Specific prime radiator area and cycle thermal efficiency variations.

(b) Pressure level and turbomachinery variations.

Figure 6. - Effect of turbomachinery rotational speed on performance. (All other initial reference conditions of table I apply).

and 150 percent, respectively. Since one design goal for this analysis was to consider use of one combined rotating unit over the net system power range from 2 to 10 kilowatts, it was required that both compressor specific speed and pressure ratio be selected so that reasonably high bearing-cavity pressures were available to the gas bearings of the rotating unit at the 2-kilowatt power level.

Rotational speed. - Results of the basic thermodynamic cycle calculations are presented in figure 6 for three rotational speeds. These speeds were chosen to be compatible with the supposition (see METHOD OF ANALYSIS) that only multiples of 400 hertz should be considered. Hence, the rotational speeds 24 000, 36 000, and 48 000 rpm (2510, 3770, and 5020 rad/sec) coupled to a four-pole alternator produce, respectively, 800, 1200, and 1600 hertz. The performance variations due to rotational speed are a direct result of the assumed turbomachinery efficiency models.

Figure 6(a) shows that cycle performance improves as rotational speed is reduced. Peak cycle efficiencies (at a compressor pressure ratio of about 2.1) show a 0.011 (4 percent) increase as rotational speed is reduced from 48 000 to 36 000 rpm (5020 to 3770 rad/sec). Reducing rotational speed from 36 000 to 24 000 rpm (3770 to 2510 rad/sec) increases cycle efficiency by 0.013 (4.6 percent). Figure 6(a) presents the effect of rotational speed, over a range of compressor pressure ratio, on turbine and compressor efficiencies and tip diameters as well as specific compressor inlet pressure. Decreasing rotational speed necessitates increasing tip diameters but results in increasing compressor efficiency, while system pressure levels decrease. Reducing shaft speed from 48 000 to 36 000 rpm (5020 to 3770 rad/sec) improves turbine efficiency only slightly over the range of compressor pressure ratio investigated, and the change from 36 000 to 24 000 rpm (3770 to 2510 rad/sec) improves turbine efficiency only at low pressure ratios (below 2.1). At the lower shaft speed, the reduced turbine efficiency improvement results from the size correlation employed in appendix B. In appendix B, it was assumed that size effects occur for radial turbines and compressors below a 6-inch (15-cm) tip diameter. As may be observed, the turbines and compressors at 24 000 rpm (2510 rad/sec) exceed 6-inch (15-cm) tip diameters above compressors pressure ratios of 1.62 and 2.03, respectively.

Choice among these speeds would be made on the basis of cycle efficiency, machinery size, and system pressure level. Although the 24 000-rpm (2510-rad/sec) solutions exhibit higher cycle efficiencies, low system pressure level might be a problem. Of course, the possibility of reducing compressor specific speed below 0.7750 tends to alleviate this drawback. However, it should also be noted that lower compressor pressure ratios are required to attain higher specific compressor inlet pressures. There is a tendency for a Brayton-cycle system to become more sensitive to temperature and/or pressure variations at low values of machinery pressure ratios. Decreasing compressor pressure ratio decreases compressor and turbine work and the temperature differences

across these components. Hence, at low compressor pressure ratio, small changes in the inlet temperatures result in a larger change in the component work and might more greatly affect the system dynamics. The solutions for the 48 000-rpm (5020-rad/sec) speed exhibit higher pressure levels but lower cycle efficiencies and smaller turbine and compressor tip diameters.

Recuperator effectiveness. - Typical effects of recuperator effectiveness on cycle performance are shown in figure 7. A range of recuperator effectiveness and compressor pressure ratio are plotted to show their overall effects on cycle thermal efficiency and specific prime radiator area. In general, increasing recuperator effectiveness increases cycle efficiency and decreases specific prime radiator area. Although increasing recuperator effectiveness decreases the average radiator temperature, the increased cycle efficiency reduces the radiator heat load, and the net result is a decrease in required radiator area.

The changes in maximum cycle efficiency with changes in recuperator effectiveness from 0.875 to 0.900, 0.900 to 0.925, and 0.925 to 0.950 were 0.011 (4.0 percent), 0.13 (4.6 percent), and 0.017 (5.7 percent), respectively. Hence, for equal increments in effectiveness, cycle efficiency increases more rapidly as effectiveness itself rises. It should be noted that the compressor pressure ratio required to produce maximum cycle efficiency at each recuperator effectiveness decreases from approximately 2.2 to

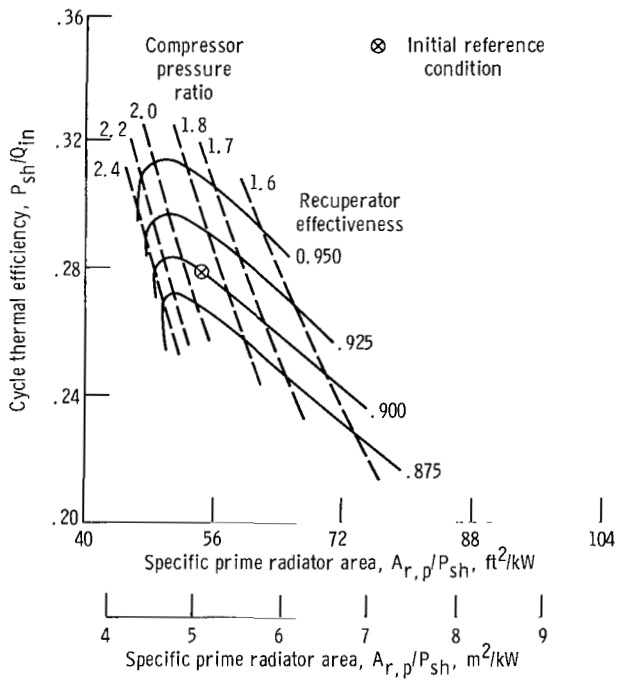


Figure 7. - Effect of recuperator effectiveness on performance. (All other initial reference conditions of table I apply.)

1.9 as recuperator effectiveness is increased from 0.875 to 0.950. In this respect, the level of recuperation will affect the selection of compressor pressure ratio and hence the machinery size and system pressure levels.

System loss pressure ratio. - Figure 8 shows the effects on cycle thermal efficiency and specific prime radiator area from varying system loss pressure ratio and compressor pressure ratio. At any value of compressor pressure ratio, increasing the system loss pressure ratio (decreasing system pressure losses) increases cycle efficiency and decreases specific radiator area.

The changes in peak system efficiency from changes in loss pressure ratio from 0.900 to 0.925 and from 0.925 to 0.950 were 0.023 (8.1 percent) and 0.021 (6.9 percent), respectively. Hence, for equal-increment increases in loss pressure ratio, the increases in cycle efficiency decrease as system losses are reduced. Those compressor pressure ratios that produce maximum cycle efficiency at each loss pressure ratio decrease from 2.1 to 1.9 with increasing system loss pressure ratio from 0.900 to 0.950. At any value of compressor pressure ratio, increasing loss pressure ratio has a negligible effect on turbine and compressor efficiencies in spite of decreases in wheel diameters and system pressure level. For example, at a compressor pressure ratio of 1.9, turbine and compressor efficiencies decrease by 0.001 and 0.002 in going from a loss pressure ratio of 0.900 to 0.950, respectively, while the specific compressor inlet pressure decreases

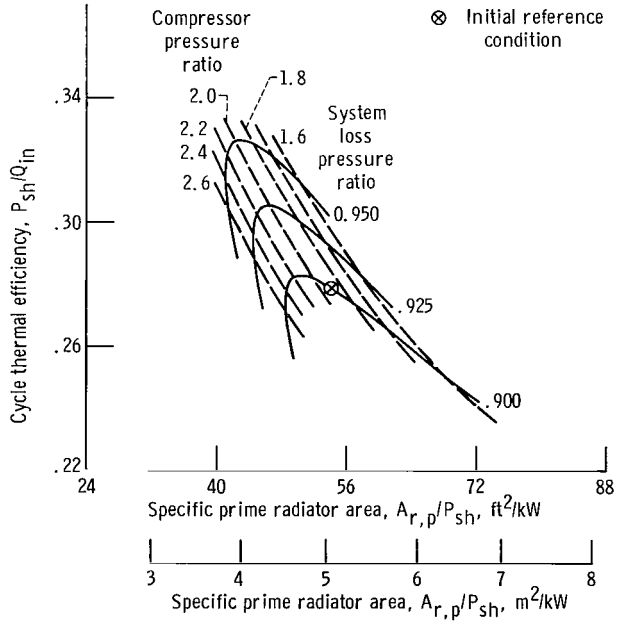


Figure 8. - Effect of loss pressure ratio on performance. (All other initial reference conditions of table I apply.)

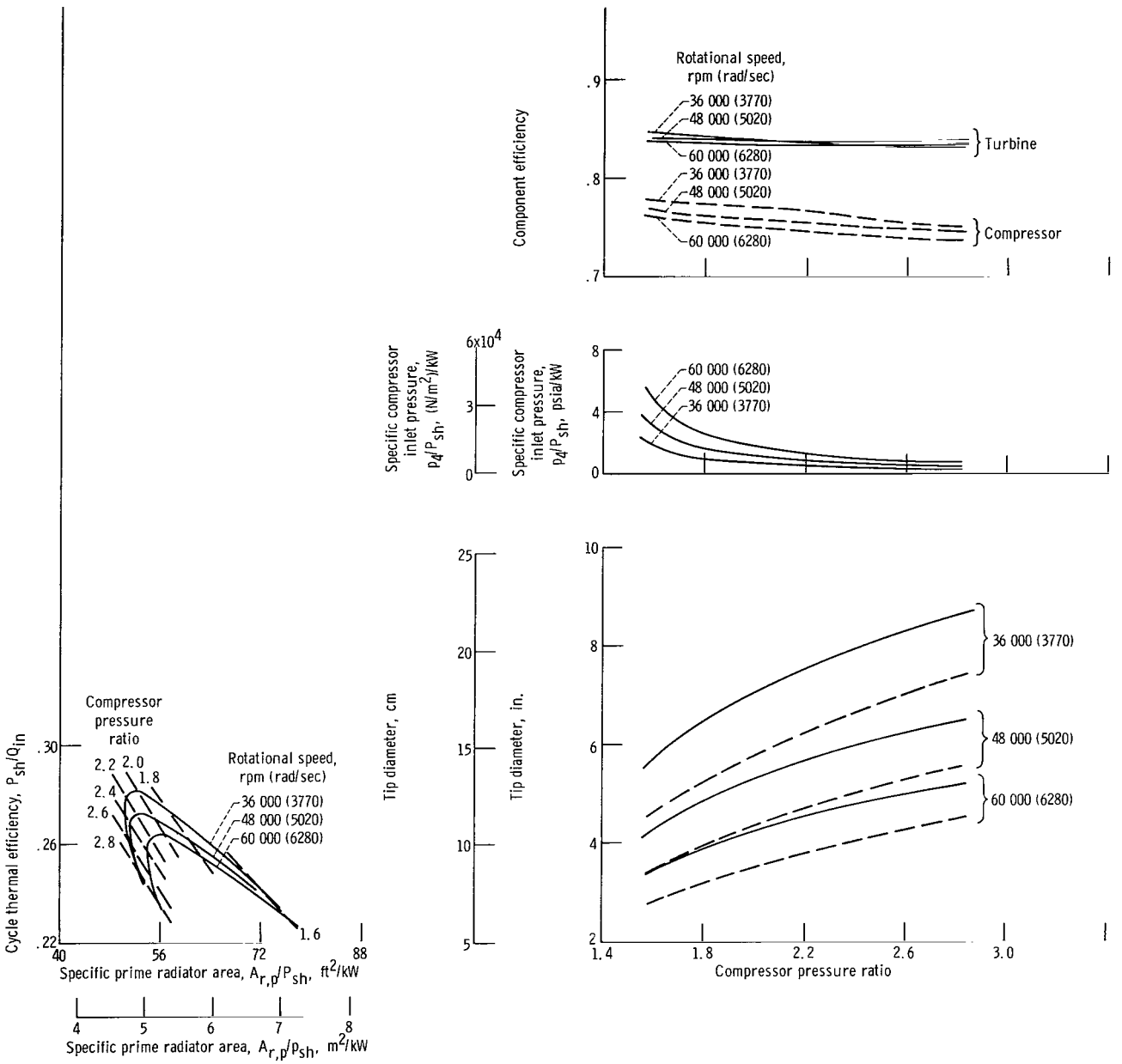


(a) Effect of rotational speed.

(b) Pressure level and turbomachinery variations.

Figure 9. - Performance at working fluid molecular weight of 39.9. (All other initial reference conditions of table I apply.)

from 2.0 to 1.6 psia per kilowatt or 13.8 to 11 newtons per meter squared kilowatt (a 20-percent decrease).

Working-fluid molecular weight. - Effects on cycle performance of the helium-xenon mixture at the molecular weight of argon are explored in figure 9 (similar to fig. 6 for molecular weight of krypton) for three rotational speeds. Figure 9(a) shows that peak cycle efficiencies occur at a compressor pressure ratio of about 2.1. Decreasing rotational speed from 60 000 to 48 000 rpm (6280 to 5020 rad/sec) increases cycle efficiency 0.008 (3 percent), and a decrease in speed from 48 000 to 36 000 rpm (5020 to 3770 rad/sec) increases cycle efficiency 0.010 (3.7 percent). Hence, at this lower molecular weight, the sensitivity of cycle efficiency to rotational speed was about the same as at the higher molecular weight.

Figure 9(b) shows the effect of changing rotational speed on turbine- and compressor-tip diameters, component efficiencies, and specific compressor inlet pressure over a range of compressor pressure ratio. The trends are similar to those for rotational speeds of 24 000, 36 000, and 48 000 rpm (2510, 3770, and 5020 rad/sec) at the molecular weight of 83.8. Because the specific compressor inlet pressure must be chosen high enough to permit successful bearing operation at the 2-kilowatt-electric system power level, specific compressor inlet pressures are greatly reduced from those at the same speed but higher molecular weight, an effect that is important. For example, for 36 000-rpm (3770-rad/sec) solutions and a compressor pressure ratio of 1.9, compressor specific inlet pressure is reduced about 65 percent from approximately 2.08 psia per kilowatt (14.3 $(kN/m^2)/kW$) at the 83.8 molecular weight to 0.72 psia per kilowatt (4.96 $(kN/m^2/kW)$ at the 39.9 molecular weight. Furthermore, specific compressor inlet pressures for the 36 000-rpm (3770-rad/sec) solutions at 83.8 molecular weight are nearly the same as those for 60 000-rpm (6280-rad/sec) solutions at 39.9 molecular weight.

Figure 10 compares the results for 36 000 rpm (3770 rad/sec) and the molecular weight of 83.8 with the results for 60 000 rpm (6280 rad/sec) and the molecular weight of 39.9. Over the range of compressor pressure ratio investigated, the higher molecular weight solutions have higher cycle efficiencies, lower prime radiator areas, and larger turbine and compressor tip diameters. In addition, maximum cycle efficiency shows an increase of 0.020, and specific radiator area shows a decrease of 6.25 square feet per kilowatt (0.58 $m^2/kW$) for the higher molecular weight. In addition to these apparent performance advantages, it was also calculated that, for the higher molecular weight, the turbine-exit impeller-root stress would be approximately half that for the lower molecular weight; this effect could be important in trying to meet the design goal of a 5-year minimum life for the system.

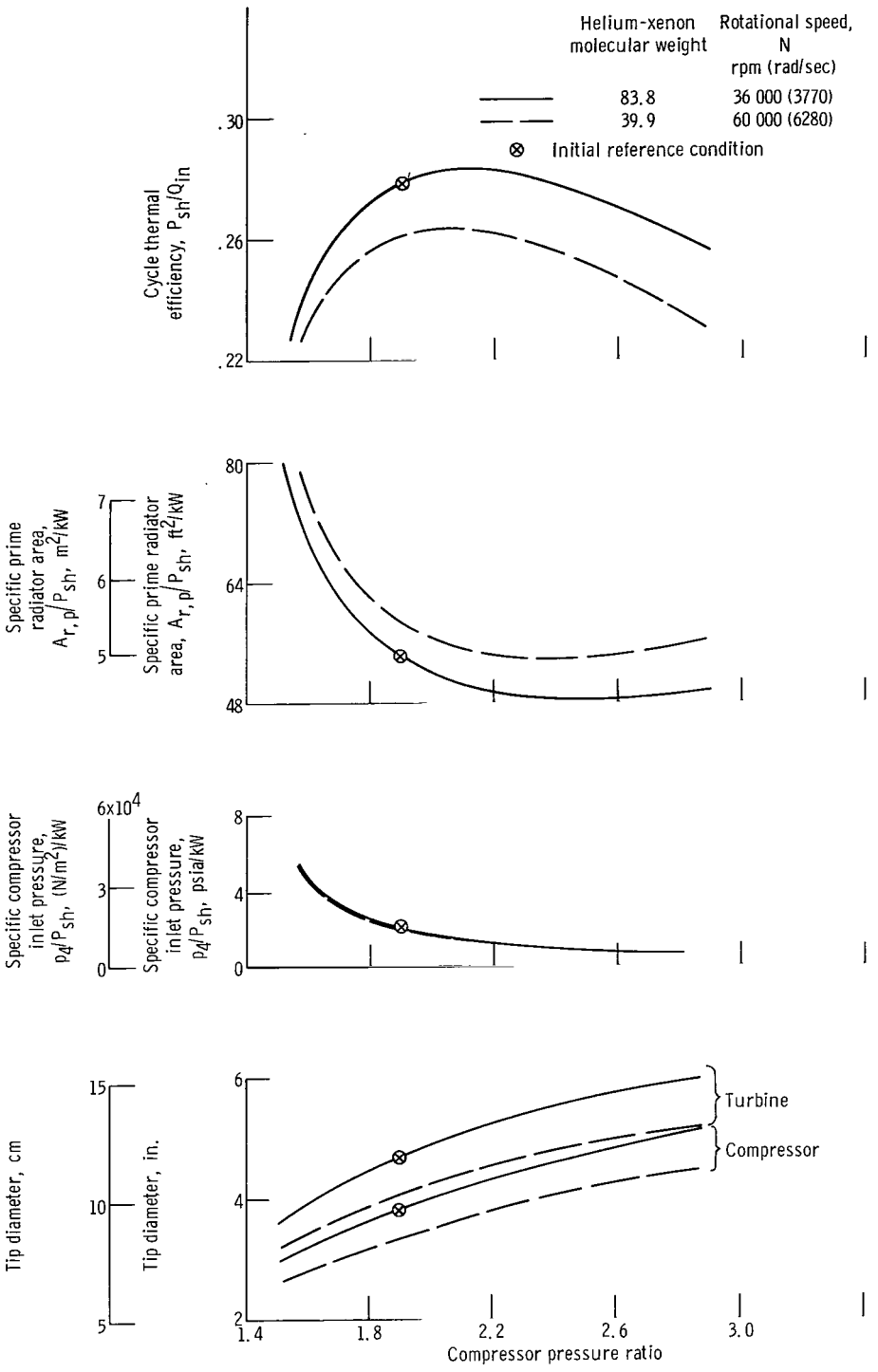


Figure 10. - Performance comparison between working fluid molecular weights. (All other initial reference conditions of table I apply.)

TABLE II. - CYCLE CONDITIONS FOR SIZE AND WEIGHT COMPARISONS

[Shaft power, 6.875 kW.]

(a) U.S. Customary Units

| Parameter[a] | Turbine inlet temperature, $T_1$, °R | | | Compressor inlet temperature, $T_4$, °R | | | Recuperator effectiveness, E | | | | Loss pressure ratio, L | | | Molecular weight, $M_w$ | |
|---|---|---|---|---|---|---|---|---|---|---|---|---|---|---|---|
| | 1860 | 1960 (b) | 2060 | 490 | 540 (b) | 588 | 0.875 | 0.900 (b) | 0.925 | 0.950 | 0.900 (b) | 0.925 | 0.950 | [c]39.9 | 83.8 (b) |
| Turbine efficiency, $\eta_t$ | 0.850 | 0.849 | 0.847 | 0.847 | 0.849 | 0.850 | 0.849 | 0.849 | 0.849 | 0.849 | 0.849 | 0.849 | 0.848 | 0.835 | 0.849 |
| Compressor efficiency, $\eta_c$ | 0.765 | 0.764 | 0.763 | 0.762 | 0.764 | 0.759 | 0.764 | 0.764 | 0.764 | 0.764 | 0.764 | 0.763 | 0.762 | 0.751 | 0.764 |
| Cycle efficiency, $\eta_{cy}$ | 0.257 | 0.279 | 0.299 | 0.317 | 0.279 | 0.235 | 0.265 | 0.279 | 0.295 | 0.313 | 0.279 | 0.304 | 0.327 | 0.261 | 0.279 |
| Prime area, $A_{r,p}$, $ft^2$ | 423 | 372 | 332 | 628 | 372 | 292 | 385 | 372 | 358 | 343 | 372 | 330 | 297 | 404 | 372 |
| Mass flow rate, m, lb/sec | 1.109 | 0.960 | 0.847 | 0.832 | 0.960 | 1.160 | 0.960 | 0.960 | 0.960 | 0.960 | 0.960 | 0.853 | 0.770 | 0.495 | 0.960 |
| Temperature, °R: | | | | | | | | | | | | | | | |
| Turbine exit, $T_2$ | 1555 | 1639 | 1723 | 1639 | 1639 | 1638 | 1639 | 1639 | 1639 | 1639 | 1639 | 1624 | 1610 | 1644 | 1639 |
| Heat-sink heat-exchanger inlet, $T_3$ | 826 | 835 | 844 | 775 | 835 | 897 | 857 | 835 | 813 | 790 | 835 | 834 | 833 | 839 | 835 |
| Compressor exit, $T_5$ | 745 | 746 | 746 | 678 | 746 | 815 | 746 | 746 | 746 | 746 | 746 | 746 | 746 | 749 | 746 |
| Heat-source heat-exchanger inlet, $T_6$ | 1474 | 1549 | 1625 | 1543 | 1549 | 1556 | 1527 | 1549 | 1572 | 1594 | 1549 | 1536 | 1524 | 1554 | 1549 |
| Pressure, psia: | | | | | | | | | | | | | | | |
| Turbine inlet, $p_1$ | 29.4 | 25.4 | 22.4 | 23.1 | 25.4 | 29.4 | 25.4 | 25.4 | 25.4 | 25.4 | 25.4 | 22.8 | 20.8 | 25.1 | 25.4 |
| Turbine exit, $p_2$ | 17.2 | 14.9 | 13.1 | 13.5 | 14.9 | 17.2 | 14.9 | 14.9 | 14.9 | 14.9 | 14.9 | 13.0 | 11.5 | 14.7 | 14.9 |
| Compressor inlet, $p_4$ | 16.0 | 13.8 | 12.2 | 12.6 | 13.8 | 16.0 | 13.8 | 13.8 | 13.8 | 13.8 | 13.8 | 12.3 | 11.1 | 13.7 | 13.8 |
| Compressor exit, $p_5$ | 30.4 | 26.3 | 23.2 | 23.9 | 26.3 | 30.4 | 26.3 | 26.3 | 26.3 | 26.3 | 26.3 | 23.4 | 21.1 | 26.0 | 26.3 |

[a]At reference conditions of table I unless otherwise noted.

[b]Initial reference conditions.

[c]Rotational speed, 60 000 rpm.

TABLE II. - Concluded. CYCLE CONDITIONS FOR SIZE AND WEIGHT COMPARISONS

[Shaft power, 6.875 kW.]

(b) SI Units

| Parameter[a] | Turbine inlet temperature, $T_1$, $^oK$ | | | Compressor inlet temperature, $T_4$, $^oK$ | | | Recuperator effectiveness, E | | | | Loss pressure ratio, L | | | Molecular weight, $M_w$ | |
|---|---|---|---|---|---|---|---|---|---|---|---|---|---|---|---|
| | 1033 | 1089 (b) | 1144 | 272 | 300 (b) | 327 | 0.875 | 0.900 (b) | 0.925 | 0.950 | 0.900 (b) | 0.925 | 0.950 | [c]39.9 | 83.8 (b) |
| Turbine efficiency, $\eta_t$ | 0.850 | 0.849 | 0.847 | 0.847 | 0.849 | 0.850 | 0.849 | 0.849 | 0.849 | 0.849 | 0.849 | 0.849 | 0.848 | 0.835 | 0.849 |
| Compressor efficiency, $\eta_c$ | 0.765 | 0.764 | 0.763 | 0.762 | 0.764 | 0.759 | 0.764 | 0.764 | 0.764 | 0.764 | 0.764 | 0.763 | 0.762 | 0.751 | 0.764 |
| Cycle efficiency, $\eta_{cy}$ | 0.257 | 0.279 | 0.299 | 0.317 | 0.279 | 0.235 | 0.265 | 0.279 | 0.295 | 0.313 | 0.279 | 0.304 | 0.327 | 0.261 | 0.279 |
| Prime area, $A_{r,p}$, $m^2$ | 40.2 | 34.6 | 30.8 | 58.3 | 34.6 | 27.1 | 35.8 | 34.6 | 33.3 | 31.8 | 34.6 | 30.6 | 27.6 | 37.5 | 34.6 |
| Mass flow rate, m, kg/sec | 0.459 | 0.436 | 0.385 | 0.378 | 0.436 | 0.526 | 0.436 | 0.436 | 0.436 | 0.436 | 0.436 | 0.387 | 0.350 | 0.225 | 0.436 |
| Temperature, $^oK$: | | | | | | | | | | | | | | | |
| Turbine exit, $T_2$ | 864 | 910 | 957 | 910 | 910 | 909 | 910 | 910 | 910 | 910 | 910 | 903 | 894 | 914 | 910 |
| Heat-sink heat-exchanger inlet, $T_3$ | 459 | 464 | 468 | 430 | 464 | 498 | 476 | 464 | 452 | 439 | 464 | 463 | 462 | 466 | 464 |
| Compressor exit, $T_5$ | 419 | 420 | 420 | 376 | 420 | 452 | 420 | 420 | 420 | 420 | 420 | 420 | 420 | 416 | 420 |
| Heat-source heat-exchanger inlet, $T_6$ | 819 | 860 | 902 | 858 | 860 | 864 | 848 | 860 | 874 | 886 | 860 | 853 | 847 | 864 | 860 |
| Pressure, $kN/m^2$: | | | | | | | | | | | | | | | |
| Turbine inlet, $p_1$ | 203 | 175 | 154 | 159 | 175 | 203 | 175 | 175 | 175 | 175 | 175 | 157 | 143 | 173 | 175 |
| Turbine exit, $p_2$ | 119 | 103 | 90 | 93 | 103 | 119 | 103 | 103 | 103 | 103 | 103 | 90 | 79 | 101 | 103 |
| Compressor inlet, $p_4$ | 110 | 95 | 84 | 87 | 95 | 110 | 95 | 95 | 95 | 95 | 95 | 85 | 77 | 94 | 95 |
| Compressor exit, $p_5$ | 210 | 181 | 160 | 165 | 181 | 210 | 181 | 181 | 181 | 181 | 181 | 161 | 145 | 179 | 181 |

[a]At reference conditions of table I unless otherwise noted.

[b]Initial reference conditions.

[c]Rotational speed, 6280 rad/sec.

## Weight Variations

Table II shows the typical cycle conditions which were used for the calculations of component and system weights. For each parameter varied, as shown in table II, the remaining cycle parameters were held at the initial reference values of table I. The shaft power was assumed to be 6.875 kilowatts.

It is recognized that the results of this section are not completely general. Particular mission requirements or other component models might alter these results. For example, more compact core geometries could reduce heat-exchanger weights, life-

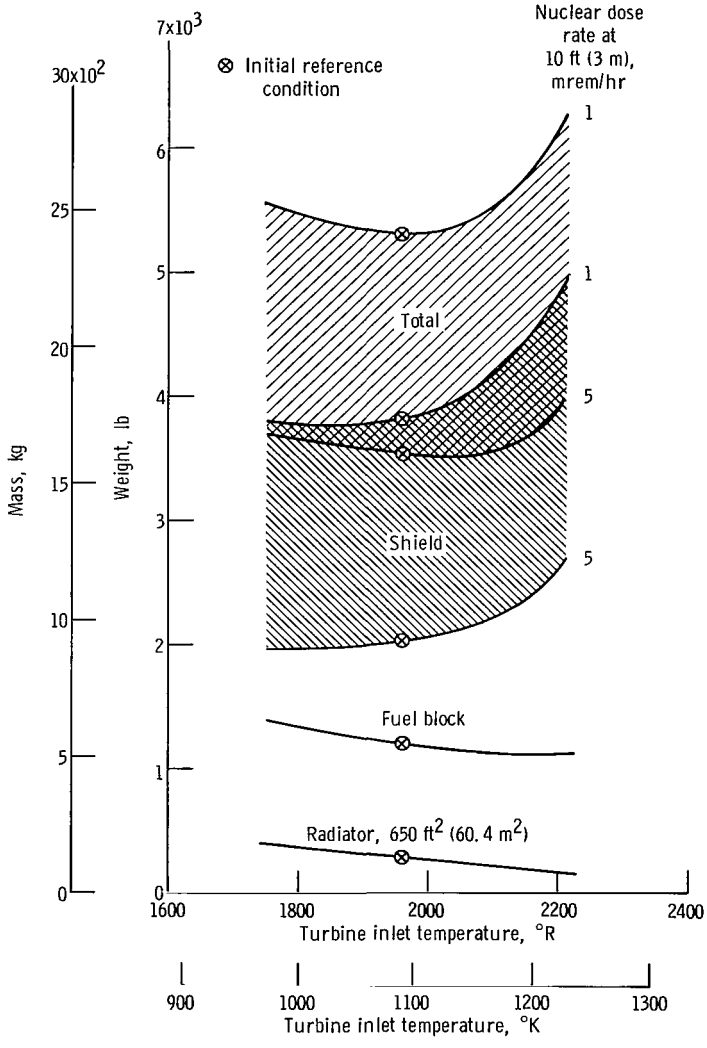


Figure 11. - Effect of turbine inlet temperature on major component weights. Gross shaft power, 6.875 kilowatts. (All other initial reference conditions of table I apply.)

support-system thermal requirements could reduce the power-system-radiator heat loads, existing vehicle structure could be used for the radiator and its weight not be charged to the power system, heat-source geometry and shielding requirements could be varied considerably, etc. Of all these possibilities, none appears to have considerable influence on this first-order selection of Brayton-cycle parameters. The assumed component models are considered to be representative of current thinking and form a reasonable basis for the preliminary selections of turbine inlet temperature, compressor inlet temperature, recuperator effectiveness, and system loss pressure ratio.

Turbine inlet temperature. - Figure 11 presents major component weights and their sum as a function of turbine inlet temperature. Radiator, fuel-block, and shield weights are presented. The radiator area has been assumed to be 650 square meters (approximately 95 $ft^2$/kW or 8.8 $m^2$/kW). This area resulted in near-minimum weight for the radiator over the range of turbine inlet temperature. Bands of shield weights and corresponding total weights are shown bounded by lines of constant nuclear dose rate of 1 and 5 millirems per hour at a distance of 10 feet (3 m) from the source. It was assumed that the remaining component weights would be unimportant with respect to these magnitudes.

The temperature range in figure 11 was extended beyond the range of initial interest in order to determine potential benefits. Both fuel-block and radiator weight decrease as turbine inlet temperature is increased in the range from $1800^\circ$ to $2200^\circ$ R ($1000^\circ$ to $1222^\circ$ K). However, the fuel block with its assumed $2460^\circ$ R ($1367^\circ$ K) temperature limitation requires increasingly large surface areas (see appendix D). This results in increasing shield weights about $1900^\circ$ R ($1056^\circ$ K). Hence, the total of these component weights exhibits minimums for dose rates of 5 and 1 millirem per hour, respectively, at approximately $2050^\circ$ and $2000^\circ$ R ($1140^\circ$ and $1110^\circ$ K).

Compressor inlet temperature. - Figure 12 presents the effect of changing radiator area and compressor inlet temperature on component weights. The lower set of curves shows that as compressor inlet temperature (radiator outlet temperature) is increased, radiator weight for a given area rapidly decreases and levels off at a given value. Shield weight (for a dose rate of 5 millirems per hour at 10 feet (3 m)), fuel-block weights, and the sum of the three component weights are presented in the top part of the figure. Decreasing compressor inlet temperature increases cycle efficiency at the expense of increasing radiator area (see Thermodynamic Variations). At each compressor inlet temperature, there is a minimum value of radiator area (i.e., the prime radiator area) required to reject the cycle heat. From a weight standpoint, a slightly larger radiator would be much lighter. For example, at $540^\circ$ R ($300^\circ$ K), the minimum-area[2] radiator is approximately 430 square feet (40 $m^2$) and 1600 pounds (720 kg). An increase in radiator

[2]The drop between the bulk liquid temperature and the radiating surface temperature is included in the radiator weight calculations. Hence, the "exact" minimum or prime area is approached as radiator weight becomes large.

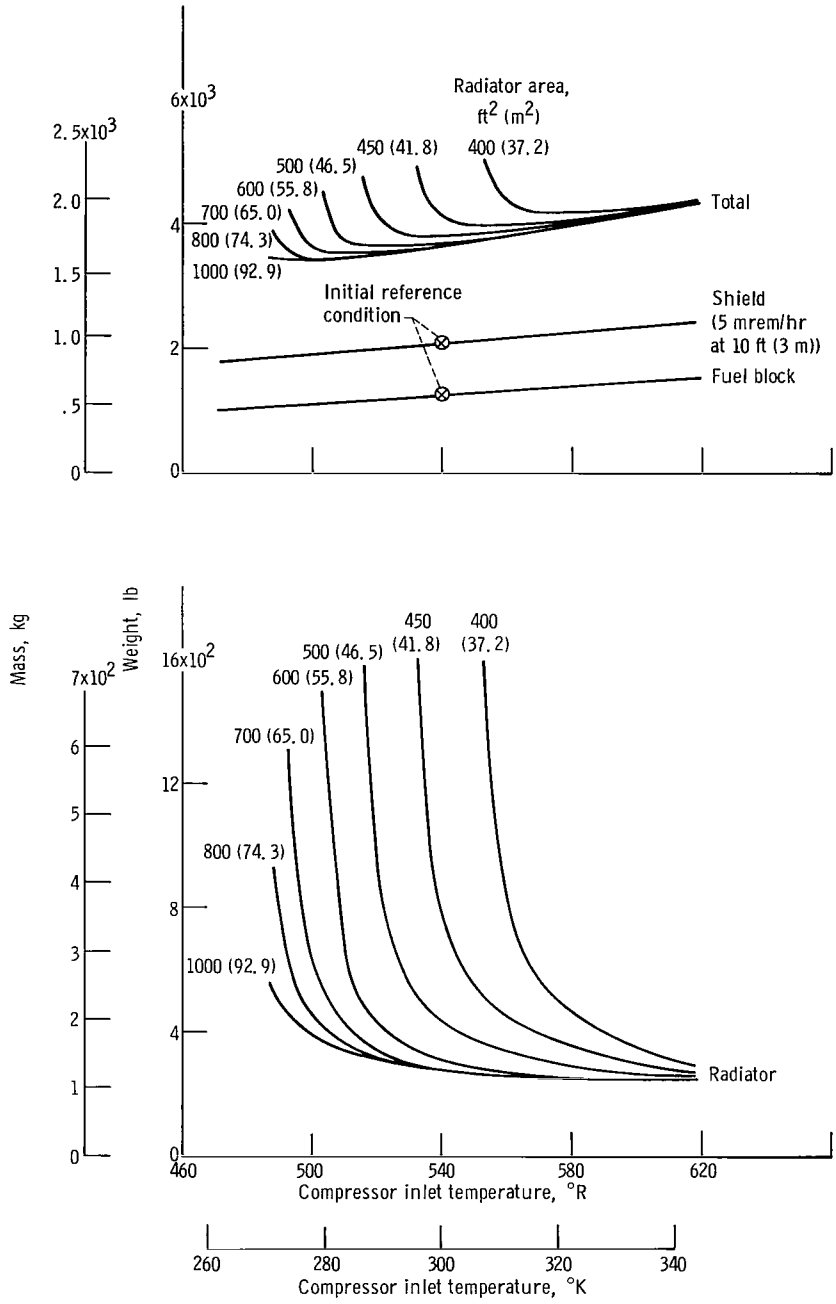


Figure 12. - Effect of compressor inlet temperature on radiator area and component weights. Gross shaft power, 6.875 kilowatts. (All other initial reference conditions of table I apply.)

area to 450 square feet (41.8 $m^2$) decreases radiator weight to 800 pounds (360 kg). For some missions, existing vehicle structure might be used as a part of the radiator structure, and, hence, area itself might be more restrictive than weight. As compressor inlet temperature is decreased, the minimum required radiator area rapidly increases. Selection of a low value for compressor inlet temperature could preclude use of the power system for some surface-area-limited applications.

The minimum total weight shown in figure 12 for 1000 square feet (92.9 $m^2$) of radiator area is 3400 pounds (1540 kg) and occurs at a compressor inlet temperature of approximately 495° R (273° K) or 45° above the assumed sink temperature. As surface

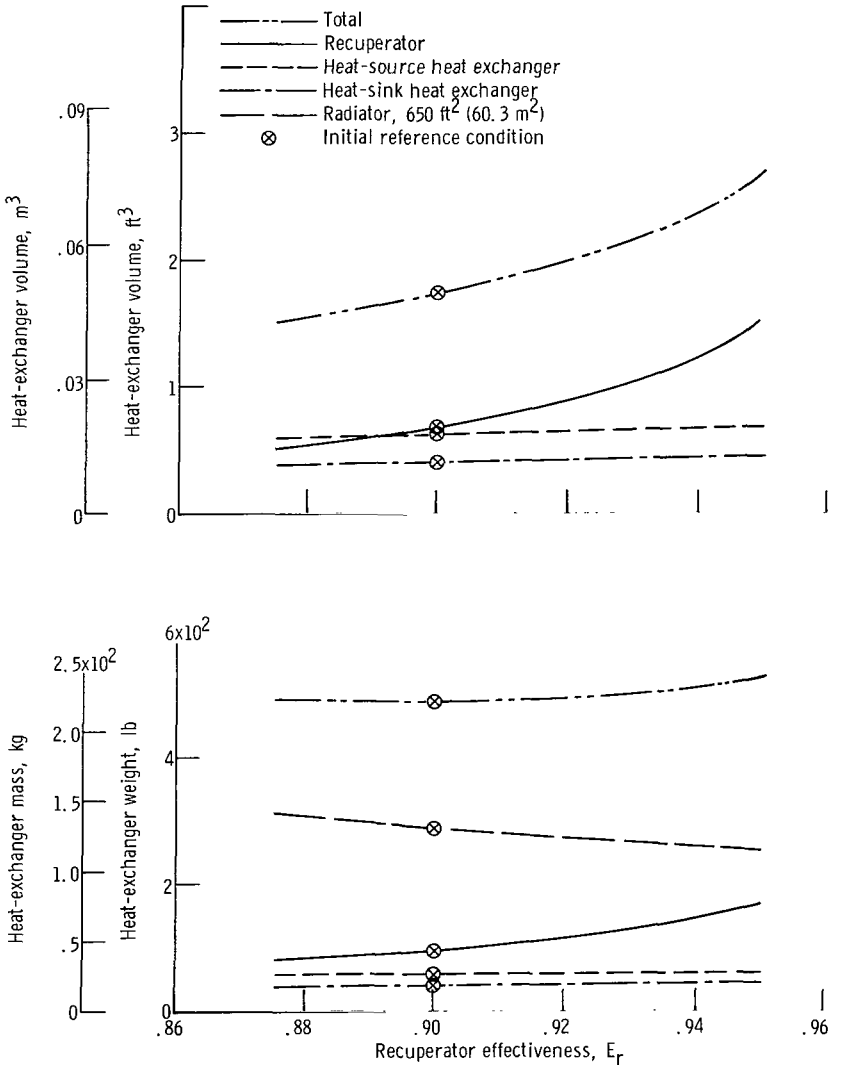


Figure 13. - Variations of heat-exchanger weights and volumes with recuperator effectiveness. Gross shaft power, 6.875 kilowatts. (All other initial reference conditions of table I apply.)

area is reduced, the compressor inlet temperature for minimum total weight increases; for example, in decreasing from 1000 to 800 to 600 to 400 square feet (92.9 to 74.3 to 55.8 to 37.2 $m^2$), the compressor inlet temperatures were 495°, 500°, 515°, and 565° R (273°, 278°, 286°, and 314° K), respectively.

Recuperator effectiveness. - Figure 13 shows the variations in weights and volumes of recuperator, heat source, and heat-sink heat exchanger over a range of recuperator effectiveness (0.87 to 0.95). In addition, radiator weight for 650 square feet (60.3 $m^2$) of radiator area is shown. Pressure-drop distributions were determined in appendix E for minimum combined heat-source, recuperator, and heat-sink heat-exchanger weights.

Increasing recuperator effectiveness increases cycle efficiency and decreases radiator weight for a fixed area but increases heat-exchanger weight and volume. For the range in effectiveness from 0.875 to 0.950, recuperator weight increases from approximately 82 to 170 pounds (37 to 77 kg), while recuperator core volume increases from

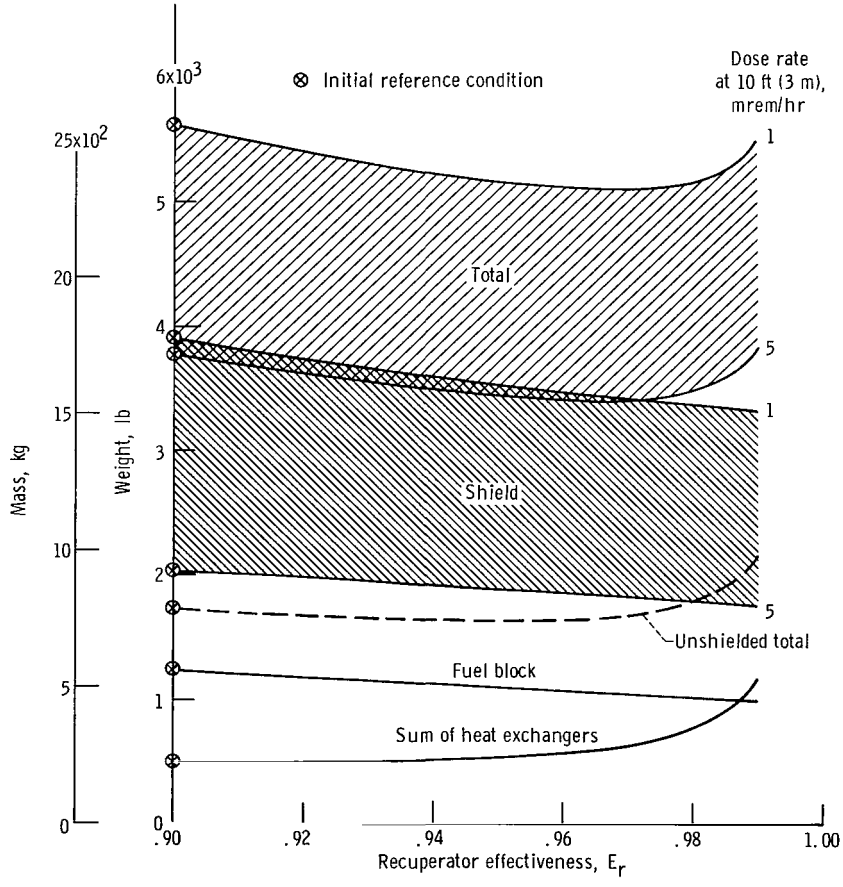


Figure 14. - Effect of recuperator effectiveness on major component weights. Gross shaft power, 6.875 kilowatts. (All other initial reference conditions of table I apply.)

approximately 0.52 to 1.52 cubic feet (0.0147 to 0.043 $m^3$). Increasing effectiveness has relatively little effect on the heat-source and heat-sink heat-exchanger weights and volumes because of the opposing effects of reduced heat loads and decreased pressure drops. The total weight for these components shows a relatively small variation over this range of recuperator effectiveness, but with an insensitive minimum of 489 pounds (222 kg) at an effectiveness of approximately 0.90. The total combined heat-source, recuperator, and heat-sink heat-exchanger volumes continually increase from about 1.5 cubic feet (0.0424 $m^3$) at an effectiveness of 0.875 to 2.68 cubic feet (0.0759 $m^3$) at 0.950. In spite of the relatively large percentage recuperator weight changes, these variations are small compared with the fuel-block weights.

Figure 14 presents variations of the major component weights and their sums with recuperator effectiveness. Because of the preponderance of heat-source weights, the range of effectiveness was extended up to 0.990 in order to establish minimum weight. Weights of fuel block, shield (for dose rates of 1 and 5 mrem/hr), combined heat exchanger, and the corresponding total of major component weights are presented along with the same total minus shield weights. The total unshielded weight has a minimum at a recuperator effectiveness of about 0.95. However, the unshielded weight does not vary appreciably for values of effectiveness from 0.90 to 0.98. The total weights for dose rates of 1 and 5 millirems per hour showed minimums at values of recuperator ef- effectiveness of approximately 0.97 and 0.96, respectively.

System loss pressure ratio. - Effects of variation in system loss pressure ratio of 0.90 to 0.95 on heat-exchanger weights and volumes are presented in figure 15. Recuperator, heat-source and heat-sink heat-exchanger weights and volumes, as well as radiator weight for 650 square feet (60.3 $m^2$) of area, and the total weights and volumes are all shown. The pressure-drop distributions as a function of total system pressure loss are presented in appendix E. Increasing loss pressure ratio increases cycle efficiency and hence reduces fuel-block and radiator weights but at the expense of heat-exchanger weights and volumes. Furthermore, small values of total system pressure loss require small component pressure drops and, in general, require more stringent designs.

Each of the three heat exchangers shows relatively small increases in weight with increasing loss pressure ratio. Addition of the radiator weight (for an area of 650 $ft^2$ or 60.3 $m^2$) to the sum of the other heat-exchanger weights results in a minimum combined weight of about 430 pounds (195 kg) at a system loss pressure ratio of 0.925. Again, these variations are small compared with the heat-source weights.

Both the recuperator and heat-sink heat exchanger show relatively small increases in volume (20 percent) with increasing loss pressure ratio, while the heat-source heat exchanger shows nearly a threefold increase in volume from a loss pressure ratio of 0.900 to 0.950. For minimum combined weight (see appendix E), the percentage pressure drop allocated to the heat-source heat exchanger varies from 3.7 percent at a loss

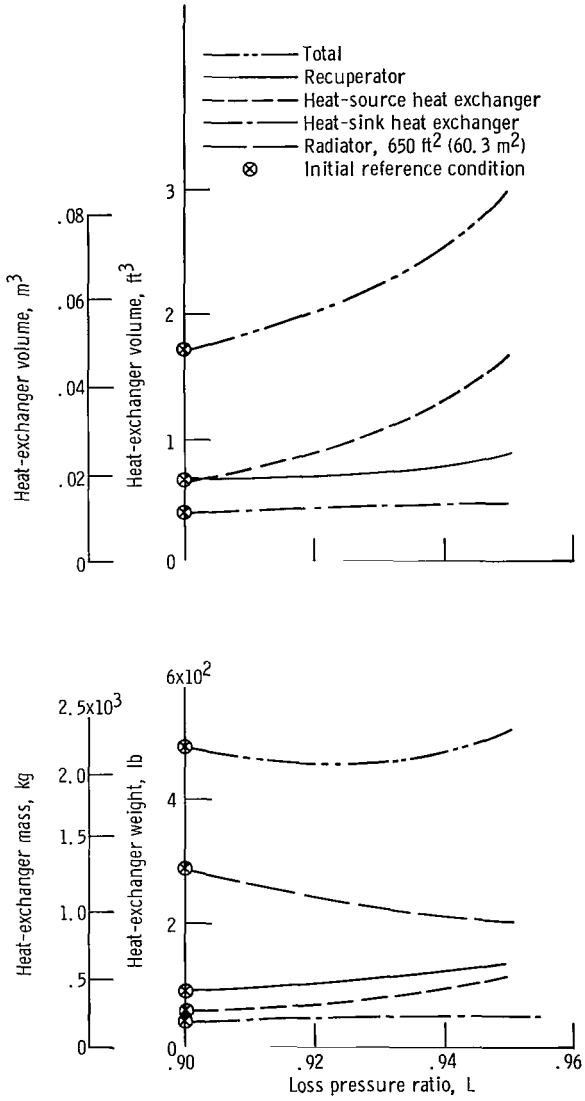


Figure 15. - Effect of loss pressure ratio on heat-exchanger weights and volumes. Gross shaft power, 6.875 kilowatts. (All other initial reference conditions of table I apply.)

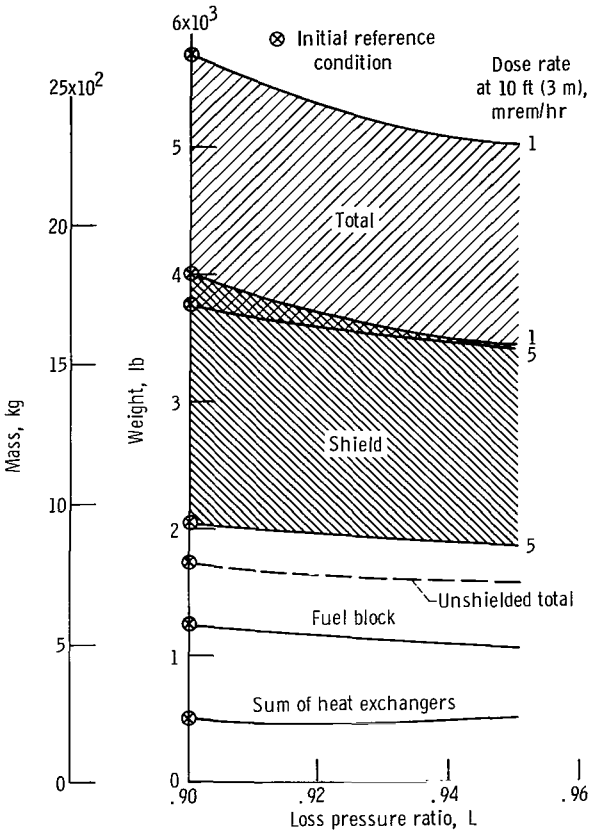


Figure 16. - Effect of loss pressure ratio on major component weights. Gross shaft power, 6.875 kilowatts. (All other initial reference conditions of table I apply.)

pressure ratio of 0.90 to 1.6 percent at a loss pressure ratio of 0.95. The total heat-exchanger volume continuously increases from about 1.7 cubic feet (0.048 $m^3$) at a loss pressure ratio of 0.90 to about 3 cubic feet (0.1 $m^3$) at 0.95.

Effects of variation in loss pressure ratio from 0.90 to 0.95 on the major component weights and their sums are presented in figure 16. The total heat-exchanger weight from figure 15, fuel-block weight, unshielded weight, a band of shield weights, and a band of the total weights are shown in figure 16. The sums show continously decreasing weight with increasing loss pressure ratio.

## Selection and Performance Estimates

Results of the parametric variations are now summarized with a selection of Brayton-cycle parameters suitable for a radioisotope power module to be designed in the electric

power range from 2 to 10 kilowatts. This is followed by performance estimates for the conceptual powerplant at 2, 6, and 10 kilowatts.

Selections. - The Brayton-cycle parameter selections and major reasons for the selections were as follows:

(1) Working-fluid molecular weight, 83.8: for the same pressure levels, this molecular weight compared with 39.9 resulted in a larger diameter turbine and compressor at lower rotational speeds and potentially higher cycle efficiency (fig. 10)

(2) Rotational speed, 36 000 rpm (3770 rad/sec): a reasonable compromise among pressure level, turbine and compressor diameter, and cycle efficiency (fig. 6)

(3) Turbine inlet temperature, $2060^{\circ}$ R ($1144^{\circ}$ K): this value resulted in high cycle efficiency, low minimum radiator area, and near-minimum total system weight (figs. 4 and 11)

(4) Compressor inlet temperature, $540^{\circ}$ R ($300^{\circ}$ K): a reasonable compromise which resulted in relatively low minimum radiator area without large penalties in total system weight (fig. 12)

(5) Recuperator effectiveness, 0.95: resulted in near-minimum total system weight and still yielded relatively compact heat-exchanger designs (figs. 13 and 14)

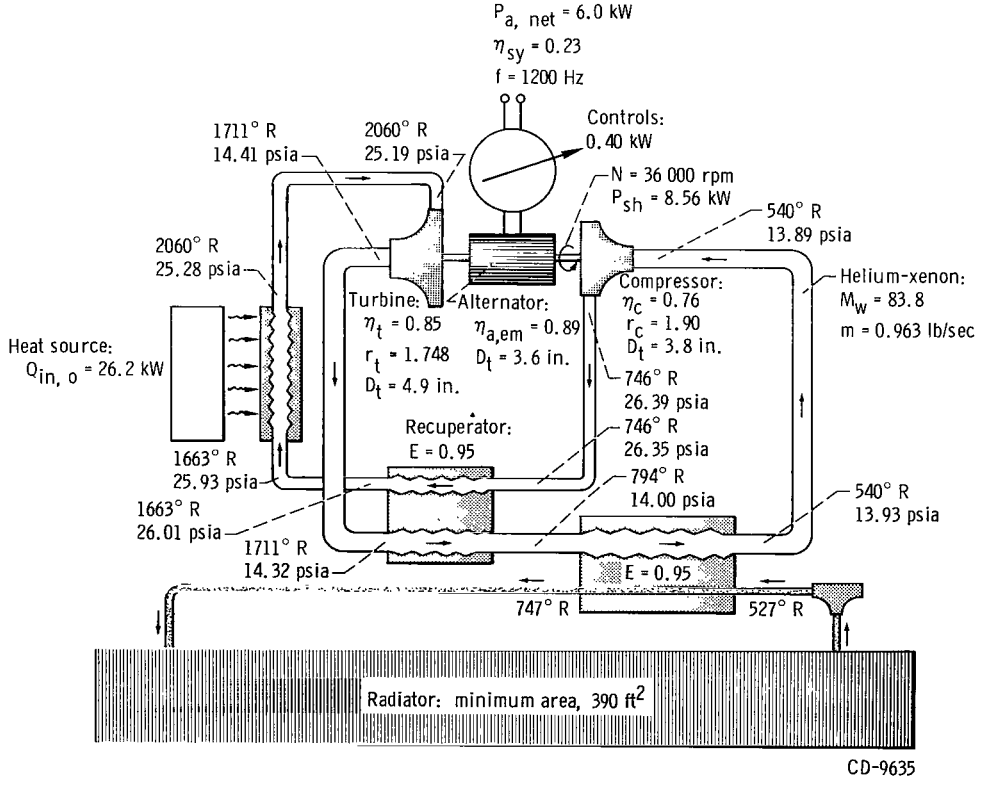


(a) U. S. Customary Units.

Figure 17. - Schematic diagram of conceptual powerplant at 6 kilowatts net power.

(6) Loss pressure ratio, 0.92: relatively low system weight and relative ease of heat-exchanger component designs (fig. 16)

(7) Compressor pressure ratio, 1.90: for the selected recuperator effectiveness and loss pressure ratio, this value should result in near-maximum efficiency and reasonable pressure levels (see figs. 5, 7, and 8 for trends)

(8) Compressor specific speed, 0.7750: with the preceding selections, this value should result in high efficiency and comparatively high bearing cavity pressure for the 2-kilowatt power level but not prohibitively high with respect to generator windage loss at the 10-kilowatt power level (appendix F)

Performance. - The preceding selections result in a cycle thermal efficiency of 0.360 and a specific compressor inlet pressure of 1.62 psi per kilowatt (11.2 $(N/m^2)/kW$). Turbine- and compressor-tip diameters were 4.9 and 3.8 inches (12.42 and 9.65 cm), respectively, while the corresponding efficiencies were predicted to be 0.85 and 0.76.

A schematic diagram of the conceptual powerplant employing the parametric selections is shown in figure 17 for a net unconditioned power output of 6 kilowatts. The alternator was assumed to be a four-pole Lundell type with a smooth 3.6-inch- (9.14-cm-) diameter rotor (see appendix F for a comparison to homopolar-inductor-type

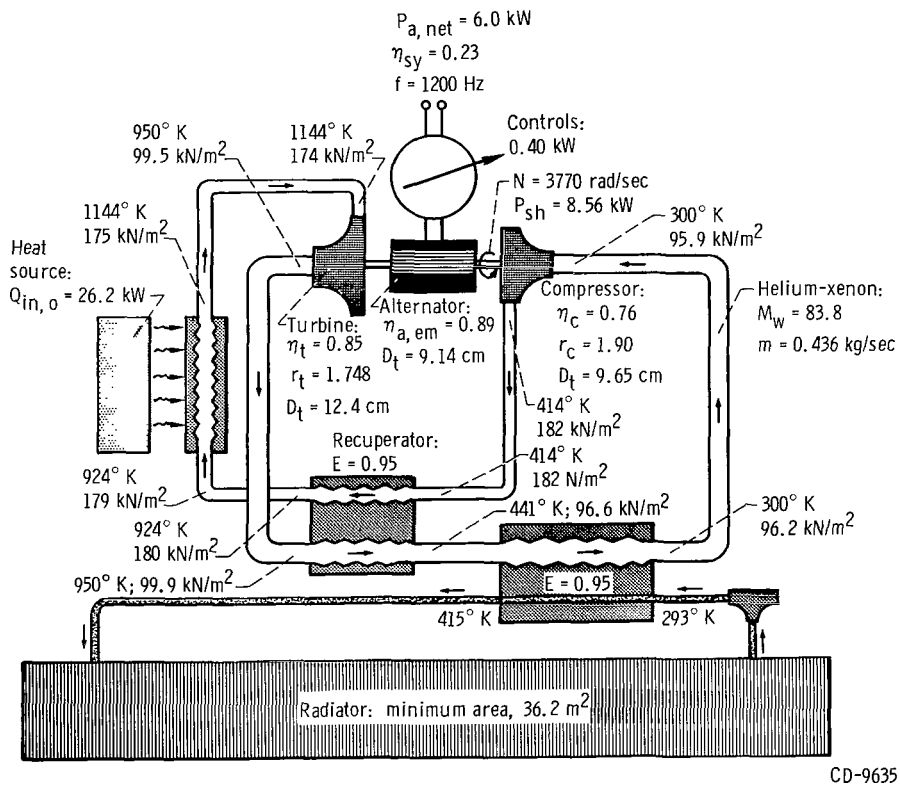


(b) SI Units.

Figure 17. - Concluded.

alternators). Resulting output frequency is 1200 hertz. The alternator was sized for 10 kilowatts of net system output and was estimated to have an electromagnetic efficiency of 0.89 at the 6-kilowatt power level. A gas mass flow rate of 0.963 pound per second (0.436 kg/sec) produces a gross shaft power of 8.56 kilowatts. Estimates of alternator windage and bearing friction and an allowance for shaft-seal losses amounted to 1.38 kilowatts; net useful shaft power is then 7.18 kilowatts. Gross alternator output is 6.4 kilowatts. An allowance of 400 watts was made for the combination of speed control, voltage regulator and exciter, parasitic load control, and liquid-coolant pump-motor power.

Required cycle thermal input is 23.8 kilowatts. An allowance of 1.2 kilowatts was made for system thermal losses, resulting in a fuel block thermal power requirement of 25.0 kilowatts at the end of the assumed 5-year mission. Allowing for isotope decay over the 5 years and 90 days (assumed launch-delay time) results in an initial thermal inventory requirement of 26.2 kilowatts. Hence, initial overall system efficiency at the 6-kilowatt net power level is 0.23.

The parametric selections result in a compressor inlet pressure of 13.89 psia (95.7 $kN/m^2$) for the 6-kilowatt net unconditioned power level. A compressor pressure ratio of 1.90 and loss pressure ratio of 0.92 results in the turbine pressure ratio of 1.748. Pressure drop distributions among the heat-exchanger components are as follows (appendix E): recuperator, 3.5 percent; heat-source heat exchanger, 2.5 percent; piping, 1.5 percent; and heat-sink heat exchanger, 0.5 percent. With the assumed heat-sink heat-exchanger effectiveness of 0.95 and capacity-rate ratio of 0.87, the minimum specific radiator area required was approximately 65 square feet per kilowatt electric or 6.04 square meters per kilowatt electric (390 $ft^2$, or 36.2 $m^2$, for 6-kW net power).

Table III presents breakdowns of the system efficiency calculations at net system power levels of 2, 6, and 10 kilowatts. The same combined rotating unit was to be used at each power level, but new heat-transfer components were employed to maintain the design parameters selected in the preceding section. The alternator was sized to produce up to 10 kilowatts of net power, while the journal bearings were sized at the 2-kilowatt power level (lowest cavity pressure). Changes in compressor and turbine efficiencies over this power range from Reynolds number effects were estimated to be small and were neglected. Hence, the compressor and turbine pressure ratios and efficiencies were assumed to be constant.

Among the parasitic losses, alternator windage dominated at the 6- and 10-kilowatt power levels, while the bearing friction was the largest of these losses at the 2-kilowatt level. For constant size and Reynolds number, alternator windage varies directly with gas pressure. The sum of the journal- and thrust-bearing frictions was estimated to be fairly constant over the power range. Seal leakage was accommodated by assuming that the compressor mass flow rate was 1 percent greater than the turbine mass flow rate.

TABLE III. - SYSTEM EFFICIENCY ESTIMATES

| | Power output, kW | | |
|---|---|---|---|
| | 2 | 6 | 10 |
| Cycle parameters: | | | |
| Initial fuel block power, kW | 10.9 | 26.2 | 41.5 |
| Thermal loss, kW | .5 | 1.2 | 1.9 |
| Cycle input power, kW | 9.9 | 23.8 | 37.7 |
| Cycle thermal efficiency | .360 | .360 | .360 |
| Gross shaft power, kW | 3.56 | 8.56 | 13.57 |
| Parasitic losses: | | | |
| Alternator windage, kW | .35 | .64 | .88 |
| Bearing friction, kW | .52 | .53 | .54 |
| Seal leakage, kW | .09 | .21 | .34 |
| Net shaft power, kW | 2.60 | 7.18 | 11.81 |
| System parameters: | | | |
| Alternator efficiency | .83 | .89 | .90 |
| Gross alternator power, kW | 2.15 | 6.40 | 10.64 |
| Radiator coolant pump power, kW | .06 | .14 | .22 |
| Control power, kW | .09 | .26 | .42 |
| Net system power (unconditioned), kW | 2.00 | 6.00 | 10.00 |
| System efficiency | 0.183 | 0.229 | 0.241 |

Alternator design point (10 kW) electromagnetic efficiency was estimated at 0.90, with a degradation to 0.89 at 6 kilowatts and 0.83 at 2 kilowatts. The remaining allowances were for the power requirements of the system itself. System efficiency was estimated to be 0.18, 0.23, and 0.24 at net system power levels of 2, 6, and 10 kilowatts, respectively.

It appears that tailoring the combined rotating unit for a specific power level rather than the range from 2 to 10 kilowatts would result in relatively small efficiency improvements. If the design were only for the 10-kilowatt level, it was estimated that about 180 watts could be saved by reducing bearing size. Hence, the sizing for the 2-kilowatt level resulted in a $1\frac{1}{4}$ percent penalty in system efficiency at the 10-kilowatt level. Conversely, if the design were only for the 2-kilowatt level, it was estimated that about 0.8 improvement in alternator electromagnetic efficiency could be obtained. Hence, the sizing for the 10-kilowatt level resulted in a 7.8 percent penalty in system efficiency at the 2-kilowatt level.

Table IV breaks down the system weight at the net system power levels of 2, 6, and 10 kilowatts. On the basis of minimum combined fuel-block and shield weight, the fuel

TABLE IV. - SYSTEM WEIGHT ESTIMATES

(a) U.S. Customary Units

| | Power output, kW | | |
|---|---|---|---|
| | 2 | 6 | 10 |
| Heat source: | | | |
| Fuel block, lb | 527 | 1226 | 2008 |
| Reentry body, lb | 150 | 345 | 565 |
| Emergency heat sink, lb | 65 | 156 | 248 |
| Subtotals: | | | |
| lb | 742 | 1727 | 2821 |
| lb/kW | 371 | 288 | 282 |
| Power conversion unit: | | | |
| Combined rotating unit, lb | 125 | 125 | 125 |
| Source heat exchanger, lb | 122 | 91 | 107 |
| Recuperator, lb | 260 | 210 | 240 |
| Sink heat exchanger, lb | 123 | 55 | 60 |
| Ducting, lb | 90 | 80 | 85 |
| Structure and insulation, lb | 200 | 160 | 180 |
| Controls, lb | 175 | 220 | 270 |
| Subtotals: | | | |
| lb | 1095 | 941 | 1067 |
| lb/kW | 548 | 157 | 107 |
| Radiator: | | | |
| Area, $ft^2$ | 180 | 540 | 900 |
| Weight: | | | |
| lb | 150 | 282 | 495 |
| lb/kW | 75 | 47 | 50 |
| Unshielded totals: | | | |
| lb | 1987 | 2950 | 4383 |
| lb/kW | 994 | 492 | 438 |
| Shield (5 mrem/hr): | | | |
| lb | 1190 | 2150 | 3050 |
| lb/kW | 595 | 360 | 305 |
| Totals: | | | |
| lb | 3177 | 5100 | 7433 |
| lb/kW | 1588 | 850 | 743 |

TABLE IV. - Concluded. SYSTEM MASS ESTIMATES

(b) SI Units

| | Power output, kW | | |
|---|---|---|---|
| | 2 | 6 | 10 |
| Heat source: | | | |
| Fuel block, kg | 240 | 556 | 912 |
| Reentry body, kg | 68 | 157 | 256 |
| Emergency heat sink, kg | 30 | 71 | 113 |
| Subtotals: | | | |
| kg | 338 | 784 | 1281 |
| kg/kW | 169 | 131 | 128 |
| Power conversion unit: | | | |
| Combined rotating unit, kg | 56.7 | 56.7 | 56.7 |
| Source heat exchanger, kg | 55.4 | 41.3 | 48.6 |
| Recuperator, kg | 118 | 95.3 | 109 |
| Sink heat exchanger, kg | 55.8 | 25.0 | 27.2 |
| Ducting, kg | 40.9 | 36.3 | 38.6 |
| Structure and insulation, kg | 90.8 | 72.6 | 81.6 |
| Controls, kg | 79.5 | 100 | 123 |
| Subtotals: | | | |
| kg | 497 | 427 | 485 |
| kg/kW | 249 | 71.2 | 48.5 |
| Radiator: | | | |
| Area, $m^2$ | 16.9 | 50.6 | 84.5 |
| Weight: | | | |
| kg | 68.1 | 128 | 225 |
| kg/kW | 34.0 | 21.4 | 22.5 |
| Unshielded totals: | | | |
| kg | 903 | 1340 | 1990 |
| kg/kW | 451 | 224 | 199 |
| Shield (5 mrem/hr): | | | |
| kg | 540 | 976 | 1385 |
| kg/kW | 270 | 163 | 139 |
| Totals: | | | |
| kg | 1440 | 2320 | 3370 |
| kg/kW | 720 | 386 | 337 |

block was assumed to have one row of capsules with each capsule void volume sized for a maximum internal pressure of 12 500 psi, or 86.1 meganewtons per square meter (appendix D). As shown in table IV, the total heat-source weight increased with increasing system power level, while the specific weight decreased. These specific weights represent from about 1/3 to 2/3 of the total unshielded system specific weights between 2 and 10 kilowatts, respectively.

The combined rotating unit was estimated to weigh 125 pounds (56.8 kg). Each of the three heat exchangers was sized for its respective heat loads, pressure levels, and percent pressure drops (all three of which varied with power level; see appendix E). Since the heat-source heat-exchanger weight was small with respect to total system weight, this component was sized for minimum volume rather than minimum weight. Presumably, the relatively small penalty (approximately 30 lb, or 13.6 kg) in the heat-source heat-exchanger weight would be more than compensated for by shield weight reduction and ease of spacing arrangements within the shielded volume.

The total weights for the power conversion unit were nearly constant for the three power levels. Opposing effects of the variations in heat load and pressure levels resulted in no major variation in heat-exchanger and hence total power conversion unit weight with power level. Specific weights, on the other hand, decreased by more than 70 percent in going from 2 to 6 kilowatts, and by an additional 32 percent in going from 6 to 10 kilowatts. The power conversion unit specific weight ranged from about 1/2 to 1/4 of the total unshielded system specific weight between 2 and 10 kilowatts, respectively.

A radiator area of 90 square feet per kilowatt electric (8.36 $m^2$/kWe) was assumed so that the radiator weights in table IV are near minimum (see appendix E). Minimum specific area requirements were approximately 65 square feet per kilowatt electric (6.04 $m^2$/kWe). Structural aspects of the radiators were not considered.

The shield weight estimates were based on a dose rate of 5 millirems per hour at a distance of 10 feet (3 m) from the isotope heat source. The absolute weight of this component increased with increasing system power output. The shield specific weights represented approximately 40 percent of the total shielded system specific weight. Both shielded and unshielded system specific weights decrease by more than a factor of 2 over the power range from 2 to 10 kilowatts.

A conceptual arrangement of the power conversion unit is shown in figure 18 for a net power output of 6 kilowatts electric. The overall package size is about 50 by 40 by 20 inches (125 by 100 by 50 cm). The hot gas from the heat-source heat exchanger enters the turbine scroll, leaves axially, and is then turned into the triangular end section of the recuperator. The flow progresses through the recuperator and heat-sink heat exchanger and is then turned back to an axial direction before entering the compressor. The compressed gases leave the compressor scroll and are ducted through the alternate passages of the recuperator and are fed back to the heat-source heat exchanger.

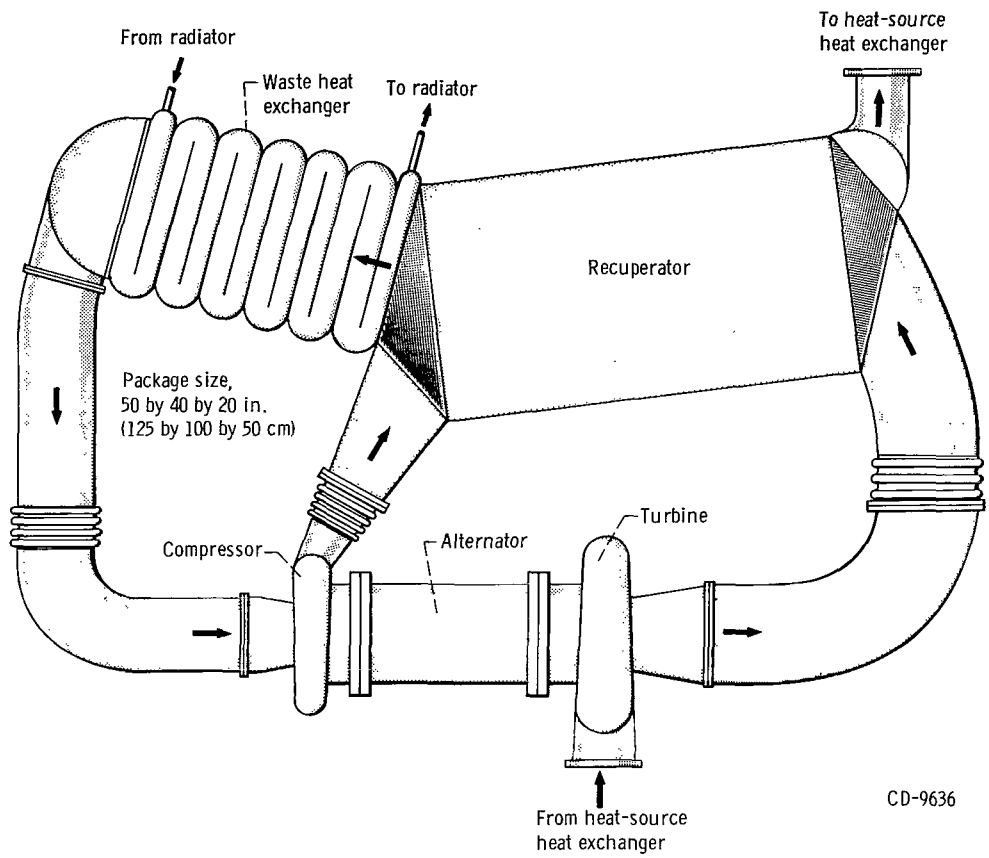


Figure 18. - Conceptual 6-kilowatt power conversion unit arrangement.

The core dimensions of the recuperator were 12.3 by 12.3 by 19.6 inches (31.2 by 31.2 by 49.8 cm) while the heat-sink heat exchanger had the dimensions 12.3 by 8.7 by 9.0 inches (31.2 by 22.1 by 22.9 cm). The combined rotating package was estimated to have a cylindrical envelope, 23 inches (58.4 cm) long and 13 inches (33 cm) in diameter.

The fuel block (see fig. 21, appendix D) for the 6-kilowatt-electric net power level required a face area of 7 square feet, or 0.65 square meter (31.8 by 31.8 in., or 80.8 by 80.8 cm) and was 3.6 inches (8.9 cm) thick. One row of capsules, each with an inner diameter of 2.40 inches (6.10 cm) was used. The heat-source heat exchanger had the dimensions 31.8 by 31.8 by 0.9 inch (80.8 by 80.8 by 2.29 cm).

## SUMMARY OF RESULTS

Parametric analysis of a conceptual plutonium 238, Brayton-cycle space powerplant yielded the following results:

1. The following major Brayton-cycle design variables were selected for a system to produce rated power from 2 to 10 kilowatts:

| | |
|---|---|
| Turbine inlet temperature, $^{o}R$ ($^{o}K$) | 2060 (1144) |
| Compressor inlet temperature, $^{o}R$ ($^{o}K$) | 540 (300) |
| Working fluid molecular weight | 83.8 |
| Shaft rotational speed, rpm (rad/sec) | 36 000 (3770) |
| Compressor pressure ratio | 1.90 |
| Compressor specific speed | 0.775 |
| System loss pressure ratio | 0.92 |
| Recuperator effectiveness | 0.95 |

2. One combined rotating unit was sized to operate over the range of rated powers from 2 to 10 kilowatts, while the gas pressure level was varied. Performance penalties for use of one combined rotating unit over this power range (compared with redesign for each power) were estimated to be small. This rotating unit consists of single-stage radial-flow turbine and compressor and a smooth-rotor four-pole alternator, all supported by hydrodynamic gas bearings. Resulting tip diameters for the turbine, alternator, and compressor were 4.9, 3.6, and 3.8 inches (12.4, 9.1, and 9.7 cm), respectively. Efficiencies for the turbine and compressor were predicted to be 0.85 and 0.76, respectively, while variations due to power level (or Reynolds number) were estimated to be small and were neglected.

3. Performance was estimated for 2, 6, and 10 kilowatts of net power output. The heat-exchanger components were resized at each power level. For this range of power, cycle thermal efficiency was 0.36, and the ratio of compressor inlet pressure to gross shaft power was 1.62 psi-kilowatt (11.18 $(kN/m^2)$-kW).

4. For minimum combined weight of heat source and nuclear shielding, radioisotope capsule void volume was sized for a maximum internal helium pressure of 12 500 psi (86.1 $MN/m^2$).

5. Overall system efficiency (the ratio of net electrical output to initial isotope thermal power), unshielded system specific weights, and shielded specific weights were estimated as follows:

| Net power, kW | Overall efficiency | Unshielded specific weight | | Shielded (5 mrem/hr) specific weight | |
|---|---|---|---|---|---|
| | | lb/kWe | kg/kWe | lb/kWe | kg/kWe |
| 2 | 0.18 | 990 | 449 | 1590 | 724 |
| 6 | .23 | 490 | 222 | 850 | 386 |
| 10 | .24 | 440 | 200 | 740 | 336 |

These weights assumed 90 square feet per kilowatt electric (8.36 $m^2$/kWe) of radiator area and resulted in near-minimum radiator weight.

6. Minimum radiator area was approximately 65 square feet per kilowatt electric (6.04 $m^2$/kWe).

7. An envelope of the power conversion unit, excluding the heat-source heat exchanger, was estimated at the 6-kilowatt power level to be 20 by 40 by 50 inches (50 by 100 by 125 cm).

Lewis Research Center,
National Aeronautics and Space Administration,
Cleveland, Ohio, January 19, 1968,
120-27-03-28-22.

# APPENDIX A

## SYMBOLS

| | |
|---|---|
| $A_{r,p}$ | prime radiator area, $ft^2$; $m^2$ |
| $A_f$ | frontal area of fuel block, $ft^2$; $m^2$ |
| a | constant in eq. (B7) |
| b | constant in eq. (B7) |
| $c_p$ | specific heat at constant pressure, Btu/(lb mass)($^oR$); J/(kg)($^oK$) |
| $C_s$ | capacity rate ratio of heat-sink heat exchanger (ref. 12), $mc_p/(mc_p)_\ell$ |
| c | axial velocity component, ft/sec; m/sec |
| $D_s$ | specific diameter[3], $\frac{D_t\left[gJ(\Delta h)_{id}\right]^{1/4}}{12\sqrt{Q}}$, dimensionless; $\left\{\frac{D_t\left[gJ(\Delta h)_{id}\right]^{1/4}}{100\sqrt{Q}}\right\}$ |
| $D_t$ | tip diameter, in.; cm |
| $E_r$ | recuperator effectiveness |
| $E_s$ | heat-sink heat-exchanger effectiveness |
| f | frequency, Hz |
| g | acceleration due to gravity, 32.2 ft/(sec$^2$)(lb mass/lb force); 9.81 m/(sec$^2$)(kg/N) |
| h | gas enthalpy, Btu/lb mass; J/kg |
| J | mechanical equivalent of heat, 778 (ft)(lb force)/Btu; (1 Nm/J) |
| $K_d$ | constant in eq. (B9), $(in.)^{-1}$; $(cm)^{-1}$ |
| $K_m$ | constant in eq. (B8) |
| L | system loss pressure ratio, $(p_1/p_{2,st})(p_4/p_5)$ |
| $L_e$ | turbine exit loss parameter, $(c_2/V_j)^2$ |
| $L_i$ | heat-source insulation loss, kW |
| $L_j$ | journal bearing friction loss, kW |
| $L_s$ | shaft seal leakage loss, kW |
| $L_t$ | thrust bearing friction loss, kW |

[3]For common usage (refs. 13 and 14, e.g.) multiply dimensionless $D_s$ by 0.420 to obtain $(sec^{1/2}/ft^{1/4})(lb\,force/lb\,mass)^{1/4}$.

| | |
|---|---|
| $L_w$ | alternator windage loss, kW |
| M* | characteristic tip Mach number |
| $M_w$ | gas molecular weight |
| m | gas mass flow rate, lb mass/hr; kg/hr |
| N | shaft rotational speed, rpm; rad/sec |
| $N_s$ | specific speed[4], $\frac{\pi N \sqrt{Q}}{30\left[gJ(\Delta h)_{id}\right]^{3/4}}$, dimensionless; $\left\{\frac{N \sqrt{Q}}{\left[gJ(\Delta h)_{id}\right]^{3/4}}\right\}$ |
| n | exponent in eq. (B7) |
| P | power, kW |
| $P_{sh}$ | gross shaft power, kW |
| $P_{sn,\,net}$ | net shaft power, kW |
| p | pressure, psi; $N/cm^2$ |
| $\Delta p/p$ | component pressure drop, percent |
| Q | volume flow rate, $ft^3/sec$; $m^3/sec$ |
| $Q_{in}$ | cycle thermal input, kW |
| R | gas constant, (ft)(lb force)/($^oR$)(lb mass); J/(kg)($^oK$) |
| Re | Reynolds number |
| r | machine pressure ratio |
| T | temperature, $^oR$; $^oK$ |
| $T_s$ | effective radiator sink temperature, 450° R; 250° K |
| $U_t$ | tip speed, ft/sec; m/sec |
| $V_j$ | ideal jet speed, ft/sec; m/sec |
| $\alpha$ | pressure drop distribution ratio, $(\Delta p/p)_{hps}/(\Delta p/p)_{lps}$ |
| $\beta$ | compressor slip factor, $gJ(\Delta h)_c/U_{t,\,c}^2$ |
| $\gamma$ | ratio of specific heats |
| $\Delta$ | difference operator |
| $\epsilon$ | surface hemispherical emittance |

[4]For common usage (refs. 13 and 14, e.g.) multiply dimensionless $N_s$ by 129 to obtain $\left[(rpm)(ft)^{3/4}/(sec)^{1/2}\right]$ (lb mass/lb force)$^{3/4}$.

| | |
|---|---|
| $\eta$ | efficiency |
| $\theta$ | area multiplication factor for radiation interchange |
| $\mu$ | gas viscosity, lb mass/(ft)(sec); kg/(m)(sec) |
| $\nu$ | turbine blade- to ideal-jet speed ratio |
| $\rho$ | gas density, lb mass/$ft^3$; $kg/m^3$ |
| $\sigma$ | Stefan-Boltzmann constant, $0.173\times10^{-8}$ Btu/(hr)($ft^2$)($^oR$)$^4$; $5.67\times10^{-8}$ J/(sec)($m^2$)($^oK$)$^4$ |

Subscripts:

| | |
|---|---|
| a | alternator |
| c | compressor |
| cr | critical |
| cy | cycle |
| em | electromagnetic |
| g | gross |
| hps | high pressure side |
| id | ideal |
| k | controls |
| $l$ | liquid |
| lps | low pressure side |
| max | maximum |
| net | net |
| o | initial |
| opt | optimum |
| p | pump |
| st | static |
| sy | system |
| t | turbine |
| 1 | turbine inlet condition |
| 2 | turbine exit condition |
| 3 | heat-sink heat-exchanger (gas side) inlet condition |

4 compressor inlet condition

5 compressor exit condition

6 heat-source heat-exchanger inlet condition

# APPENDIX B

## RADIAL TURBOMACHINERY EFFICIENCY MODELS

By dimensional analysis, reference 15 shows that only four parameters are required to describe completely the performance of compressible flow turbomachinery, provided that complete physical similarity can be maintained. Quoting from reference 15, "Complete physical similitude implies (1) geometrical similitude, which means that the linear dimension ratios are everywhere the same, that is, shapes are similar regardless of size; (2) kinematic similitude, which means that velocity ratios are the same, i.e., the velocity triangles representing flow conditions are similar; and (3) dynamic similitude, which means that the ratios of the different forces are everywhere the same. For fluid flow, the streamlines are everywhere similar." In practice, complete similitude is difficult to attain. This is especially true for small machinery where manufacturing techniques necessary to attain similar clearance ratios are not practical. (These techniques could be achieved but currently do not warrant the cost.)

The empirical models of this analysis were based on the four similarity parameters of references 13 and 14 with minor modifications and the inclusion of a "size effect." Hence, the total efficiencies of both turbine and compressor were assumed to be functions only of specific speed, specific diameter, Reynolds number, characteristic tip Mach number, and tip diameter, or expressed functionally,

$$\eta = f(N_s, D_s, Re, M^*, D_t) \tag{B1}$$

The model assumed that the compilation of best efficiency points for radial-flow turbines and compressors as a function of specific speed, presented in reference 16, represented the maximum obtainable efficiency, that is, the efficiency obtainable when the remaining parameters were at their optimum values or beyond their range of influence. Hence, from reference 16,

$$\eta = \eta_{max} = f(N_s) \tag{B2}$$

for

$$Re \geq (Re)_{cr}$$

$$M^* \leq (M^*)_{cr}$$

$$D_t \geq (D_t)_{cr}$$

$$D_s = (D_s)_{opt}$$

It was assumed that the optimum specific diameter would result from the specification of rotational speed and a blade- to ideal-jet speed ratio of 0.70 for the turbine, and rotational speed and a 0.85 value of slip factor for the straight radial-bladed compressor. Symbolically, this is represented as

$$(D_s)_{opt} = f(D_t) \tag{B3}$$

$$D_t = \frac{720\, U_t}{\pi N}; \quad \left(D_t = \frac{200\, U_t}{N}\right) \tag{B4}$$

where for a turbine,

$$U_{t,t} = \sqrt{\nu_j}$$

$$= 0.70 \sqrt{2gJ(\Delta h)_{t,\,id,\,st}} \tag{B5}$$

and for a compressor,

$$U_{t,c} = \sqrt{\frac{gJ}{\beta}(\Delta h)_c}$$

$$= \sqrt{\frac{gJ}{0.85}(\Delta h)_c} \tag{B6}$$

A critical Reynolds number of $10^7$ was assumed and efficiency corrections were assumed to follow the general form (ref. 15)

$$\eta = 1 - (1 - \eta_{max})\left[a + b\left(\frac{10^7}{Re}\right)^n\right] \tag{B7}$$

for $Re < 10^7$. Mach number (or pressure ratio, since the two are related) effects were

assumed to be linear above critical values and have the general form

$$\Delta\eta = - K_m(M^* - M^*_{cr}) \tag{B8}$$

for $M^* > M^*_{cr}$. A critical tip diameter of 6 inches (15 cm) was assumed with efficiency corrections empirically fitted to

$$\Delta\eta = K_d(6.0 - D_t); \quad \left[\Delta\eta = - K_d(15.24 - D_t)\right] \tag{B9}$$

for $D_t < 6.0$ $(D_t < 15.24)$.

From the results of the 6-inch (15-cm) turbine and compressor investigations (ref. 6), the following coefficients were determined for equation (B7) (the effect of Reynolds number). For the turbine,

$$a = 0.3 \quad b = 0.7 \quad n = 0.20$$

and for the compressor,

$$a = 0, \quad b = 1.0, \quad n = 0.06$$

Comparisons among analytical and experimental results of references 5, 13, 14, and 17 led to selection of the constants of the Mach number correction (eq. (B8)) for the compressor. These were $K_m = 0.075$ and $M^*_{cr} = 0.5$. For the Mach number effect on turbines, the analytical results of reference 17 were employed. The constants were $K_m = 0.070$ and $M^*_{cr} = 0.25$ for the range of $0.25 \leq M^* \leq 0.75$, and $K_m = 0.320$ and $M^*_{cr} = 0.75$ for $M^* > 0.75$. Using the preceding corrections and the peak performance results shown in table V, the remaining efficiency differences were allocated to the "size effect." The resulting coefficients were

$$K_d = 0.0125; \quad \left[K_d = 0.00403\right]$$

for compressors with $D_t < 6.0$ $(D_t < 15.24)$ and

$$K_d = 0.0085; \quad \left[K_d = 0.00335\right]$$

for turbines with $D_t > 6.0$ $(D_t > 15.24)$.

The procedure then in calculating a turbine or compressor efficiency was to assume a rotational speed and a specific speed and to determine the maximum efficiency from the

empirical prediction of reference 16 (eq. (B2)). Then, this calculated efficiency was corrected for Reynolds number (eq. (B7)), Mach number (eq. (B8)), and size (eqs. (B4) and (B9)) in that order.

TABLE V. - COMPARISON OF RADIAL-FLOW TURBOMACHINERY AT PEAK EFFICIENCY

| Parameter | Turbines | | Compressors | |
|---|---|---|---|---|
| Tip diameter, $D_t$: | | | | |
| in.[2] | 6.02 | 4.59 | 6.0 | 3.2 |
| cm | 15.3 | 11.7 | 15.2 | 8.12 |
| Total pressure ratio | 1.565 | 1.555 | 2.33 | 2.00 |
| Static pressure ratio | 1.610 | 1.605 | -------- | -------- |
| Total efficiency | 0.88 | 0.864 | 0.745 | [a]0.750 |
| Static efficiency | 0.83 | 0.810 | -------- | -------- |
| Specific speed, $N_s$ | 0.688 | 0.734 | 0.631 | 0.691 |
| Specific diameter, $D_s$ | 2.95 | 2.78 | 3.89 | 3.46 |
| Reynolds number, Re | $3.5\times10^5$ | $4.4\times10^5$ | $1.39\times10^6$ | $3.12\times10^6$ |
| Tip Mach number, M* | 0.582 | 0.579 | 1.104 | 0.956 |
| Exit loss parameter, $L_e$ | 0.059 | 0.064 | -------- | -------- |
| Slip factor, $\beta$ | ------- | ------- | 0.89 | 0.93 |

[a]Estimated as 0.05 lower than measured thermal efficiency.

# APPENDIX C

## CYCLE CALCULATION PROCEDURE

A digital machine computer code was constructed to analyze the thermodynamics of the Brayton cycle system utilizing the efficiency models presented in appendix B. The equations and procedure of this analysis are presented.

The input parameters basically were those listed in table I. For gas properties, the analysis assumed perfect gas relations. Compressor specific work was calculated from

$$(\Delta h)_c = \frac{c_p T_4}{\eta_c}\left[\left(\frac{p_5}{p_4}\right)^{(\gamma-1)/\gamma} - 1\right] \tag{C1}$$

where

$$c_p = \frac{\gamma}{\gamma - 1}\frac{R}{J}\left(\gamma = \frac{5}{3}\right) \tag{C2}$$

and

$$R = \frac{1545}{M_w}; \qquad \left[R = \frac{8317}{M_w}\right] \tag{C3}$$

Initially, an arbitrary value was assumed for $\eta_c$, while $T_4$ and $p_5/p_4$ were specified in the input. The pressure ratio available to the turbine was given by

$$\frac{p_1}{p_{2,\,st}} = L\left(\frac{p_5}{p_4}\right) \tag{C4}$$

and the turbine specific work was determined from

$$(\Delta h)_t = \eta_{t,\,st} c_p T_1 \left[1 - \left(\frac{p_1}{p_{2,\,st}}\right)^{-(\gamma-1)/\gamma}\right] \tag{C5}$$

Initially, efficiency was an assumed value. For a fixed gross shaft power, the cycle mass flow rate was given by

$$M = \frac{3415P_{sh}}{(\Delta h)_t - (\Delta h)_c}; \qquad \left[M = \frac{1550P_{sh}}{(\Delta h)_t - (\Delta h)_c}\right] \tag{C6}$$

The next steps sized the turbine and compressor and computed the component efficiency by iterating until the assumed efficiencies agreed with the calculated efficiencies within ±0.0005. Compressor tip speed was calculated from

$$U_{t,c} = \sqrt{\frac{gJ}{\beta}(\Delta h)_c} \tag{C7}$$

and tip diameter from

$$D_{t,c} = \frac{720U_{t,c}}{\pi N} = \frac{U_{t,c}}{100N} \tag{C8}$$

With rotational speed and compressor specific speed assigned, the compressor characteristic volume flow (inlet) was obtained from

$$Q_4 = \left(\frac{30N_{s,c}}{\pi N}\right)^2 \left[gJ\eta_c(\Delta h)_c\right]^{3/2}; \qquad Q_4 = \left(\frac{N_{s,c}}{N}\right)^2 \left[gJ\eta_c(\Delta h)_c\right]^{3/2} \tag{C9}$$

Hence, the inlet density and pressure were evaluated as

$$\rho_4 = \frac{m}{3600Q_4} \tag{C10}$$

and

$$p_4 = \frac{\rho_4 RT_4}{144}; \qquad \left[p_4 = \rho_4 RT_4\right] \tag{C11}$$

The characteristic tip Mach number (ratio of tip speed to the critical speed of sound at the inlet) and Reynolds number were obtained from

$$M_c^* = \frac{U_{t,c}}{\sqrt{\frac{2\gamma}{\gamma + 1} gRT_4}} \tag{C12}$$

and

$$Re_c = \frac{\rho_4 U_{t,c} D_{t,c}}{12\mu_4}; \quad \left[ Re_c = \frac{\rho_4 U_{t,c} D_{t,c}}{100 u_4} \right] \tag{C13}$$

Fluid viscosities (as a function of temperature) and maximum component efficiencies (as a function of specific speed) were handled as tables which were interpolated in appropriate subroutines. With the preceding calculations used as input, an efficiency for the compressor was calculated from equation (B7).

Turbine tip speed and diameter were calculated from

$$U_{t,t} = \nu_j \tag{C14}$$

and

$$D_{t,t} = \frac{720 U_{t,t}}{\pi N}; \quad \left[ D_{t,t} = \frac{U_{t,t}}{100N} \right] \tag{C15}$$

where

$$V_j = \sqrt{2qJ(\Delta h)_{t,\,id,\,st}} \tag{C16}$$

and

$$(\Delta h)_{t,\,id,\,st} = \frac{(\Delta h)_t}{\eta_{t,\,st}} \tag{C17}$$

The turbine characteristic volume flow $Q_{2,\,st}$ (exit static conditions) was developed from the following relations:

$$T_2 = T_1 - \frac{(\Delta h)_t}{c_p} \tag{C18}$$

$$T_{2,\,st} = T_2 - \frac{L_e(\Delta h)_{t,\,id,\,st}}{c_p} \tag{C19}$$

$$\frac{p_4}{p_{2,\,st}} = \frac{\alpha - 1 + \sqrt{(\alpha - 1)^2 + 4\alpha L}}{2\alpha} \tag{C20}$$

where $\alpha \equiv (\Delta p/p)_{hps}/(\Delta p/p)_{lps}$

$$p_{2,\,st} = \frac{p_4}{\dfrac{p_4}{p_{2,\,st}}} \tag{C21}$$

$$\rho_{2,\,st} = \frac{144 p_{2,\,st}}{RT_{2,\,st}}; \qquad \left[\rho_{2,\,st} = \frac{p_{2,\,st}}{RT_{2,\,st}}\right] \tag{C22}$$

$$Q_{2,\,st} = \frac{m}{3600\rho_{2,\,st}} \tag{C23}$$

The parameters L, $L_e$, and $\alpha$ were input quantities.

Turbine total efficiency was related to its static efficiency by

$$\eta_t = \frac{\eta_{t,\,st}}{1 - L_e} \tag{C24}$$

Turbine specific speed was calculated from

$$N_{s,\,t} = \frac{\pi N \sqrt{Q_{2,\,st}}}{30\left[gJ\,\dfrac{(\Delta h)_t}{\eta_t}\right]^{3/4}}; \qquad \left[N_{s,\,t} = \frac{N \sqrt{Q_{2,\,st}}}{\left[gJ\,\dfrac{(\Delta h)_t}{\eta_t}\right]^{3/4}}\right] \tag{C25}$$

The characteristic blade tip Mach number and Reynolds number based on inlet conditions were evaluated from

$$M_t^* = \frac{U_{t,t}}{\sqrt{\frac{2\gamma}{\gamma + 1} gRT_1}} \tag{C26}$$

and

$$Re_t = \frac{\rho_1 U_{t,t} D_{t,t}}{12\mu_1}; \qquad \left[ Re_t = \frac{p_1 U_{t,t} D_{t,t}}{100\mu} \right] \tag{C27}$$

where

$$p_1 = p_{2,st}\left(\frac{p_1}{p_{2,st}}\right) \tag{C28}$$

and

$$\rho_1 = \frac{144 p_1}{RT_1}; \qquad \left[ \rho_1 = \frac{p_1}{RT_1} \right] \tag{C29}$$

The preceding quantities and the methods of appendix B were used to estimate turbine efficiency. As indicated, this procedure was iterated until component efficiency was within ±0.0005. The remaining cycle temperatures and the cycle thermal efficiency were then calculated from

$$T_5 = T_4 + \frac{(\Delta h)_c}{c_p} \tag{C30}$$

$$T_3 = T_2 - E_r(T_2 - T_5) \tag{C31}$$

$$T_6 = T_5 + E_r(T_2 - T_5) \tag{C32}$$

and

$$\eta_{cy} = \frac{3415P_{sh}}{mc_p(T_1 - T_6)} \equiv \frac{P_{sh}}{Q_{in}}; \qquad \left[\eta_{cy} = \frac{1550P_{sh}}{mc_p(T_1 - T_6)}\right] \tag{C33}$$

The liquid radiator temperatures were determined from the assigned values of $E_s$, $C_s$, and

$$T_{4,\ell} = T_3 - \frac{T_3 - T_4}{E_s} \tag{C34}$$

$$T_{3,\ell} = T_{4,\ell} + C_s(T_3 - T_4) \tag{C35}$$

where

$$C_s = \frac{mc_p}{(mc_p)_\ell}$$

The required prime radiator area $A_{r,p}$ was approximated from the following relation from reference 11

$$A_{r,p} = \frac{(mc_p)_\ell}{4\sigma\epsilon T_s^3}\left[\ln\frac{(T_{3,\ell} - T_s)(T_{4,\ell} + T_s)}{(T_{4,\ell} - T_s)(T_{3,\ell} + T_s)} - 2\left(\tan^{-1}\frac{T_{3,\ell}}{T_s} - \tan^{-1}\frac{T_{4,\ell}}{T_s}\right)\right] \tag{C36}$$

where the radiator wall temperature drop has been neglected.

The output from this procedure included all cycle temperatures, compressor and turbine pressures, overall geometry of the turbine and compressor, with characteristic numbers plus cycle thermal efficiency and prime liquid radiator area requirements.

# APPENDIX D

# HEAT SOURCE ANALYSIS

by John L. Klann, Leonard Soffer, and Gerald J. Barna

Gross shielding approximations and factors affecting fuel block geometry and weight are presented.

## Shielding

Approximate shield thicknesses which were calculated in the analysis are shown in figure 19 as a function of the initial plutonium 238 thermal inventory and two radiation dose rates. These thicknesses were obtained by an unpublished approximate technique which was intended for use in demonstrating trends. The fuel block was treated as a point source, and self-shielding was neglected. The radiation dose distribution at the manned compartment was assumed to be 90 percent gammas and 10 percent neutrons in order to approximate minimum shield weight.

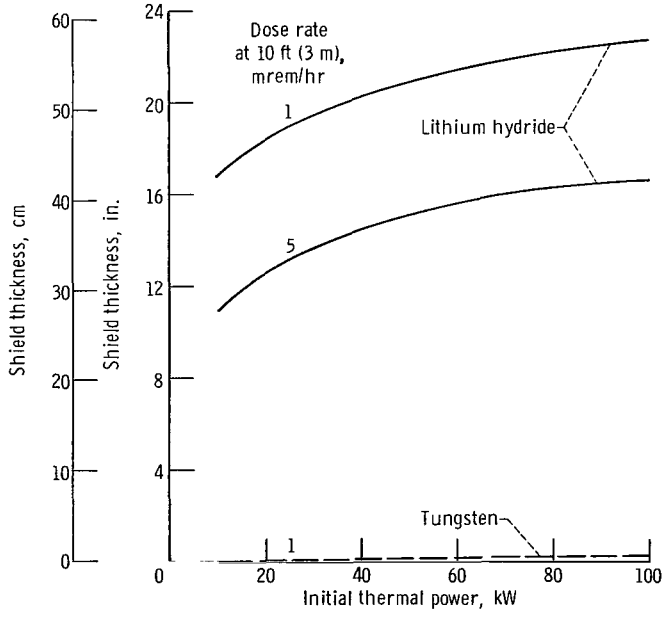


Figure 19. - Approximate shield thickness as function of initial plutonium 238 thermal inventory and dose rate.

Lithium hydride was used for shielding the gamma and neutron radiation. Over the range of initial radioisotope thermal inventory of interest for this analysis (approximately 10 to 40 kW), the shield thicknesses varied from about 11 to 14.5 inches (28 to 37 cm) for a dose rate of 5 millirems per hour at a distance of 10 feet (3 m) and from about 17 to 20.5 inches (43 to 52 cm) for a dose rate of 1 millirem per hour. Only the lower dose rate required tungsten shielding (approximately 0.1 in., or 0.25 cm) for the allowed gamma dose.

Figure 20 presents the side and front (corresponding to the side of the large face of the fuel block facing the power system) shield weights, calculated from the shield thicknesses of figure 19, as functions of the two dose rates and the initial radioisotope inventory. The shield geometry was that idealized in figure 2. The fuel block was assumed to be a point source located 7 inches (17.8 cm) behind the front shield. A fuel block specific area density ($A_F/Q_{in,o}$) of 0.162 square foot per kilowatt (0.015 $m^2$/kW) was assumed. Hence, for a given thermal inventory, the fuel block frontal area was determined. With a 1-inch (2.54-cm) clearance between the fuel block and side shields and 6 inches (15.2 cm) of shield overhang beneath the fuel block, the dimensions of the four shield pieces and their weights were then determined. Radiation scattering was not considered in determining the shield weight. A comparison was made between the weights shown in figure 20 and those calculated by more rigorous methods. The curves resulted in a total shield weight which was 10 to 20 percent heavier than those which were more exact.

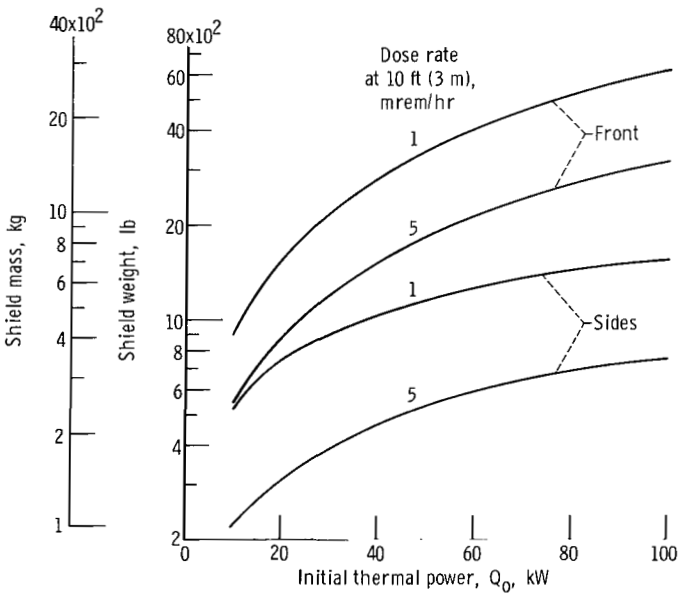


Figure 20. - Shield weights for assumed geometry as function of initial power and dose rate.

Over the range of parameters investigated in this analysis, fuel block specific area densities varied from 0.22 to 0.38 square foot per kilowatt (0.020 to 0.035 $m^2$/kW). Hence, the shield weights were obtained indirectly from figure 20. The front shield weight was scaled directly as the ratio of the calculated fuel block specific area density to the reference value of the figure (0.162 $ft^2$/kW, or 0.015 $m^2$/kW) and summed with the uncorrected combined side shield weight.

## Fuel Block

The concept and methods of reference 2 were employed in a digital computer program to calculate the geometry and weight of the fuel block. A schematic diagram of the 6-kilowatt-electric powerplant fuel block is shown in figure 21. Nine rows of fuel

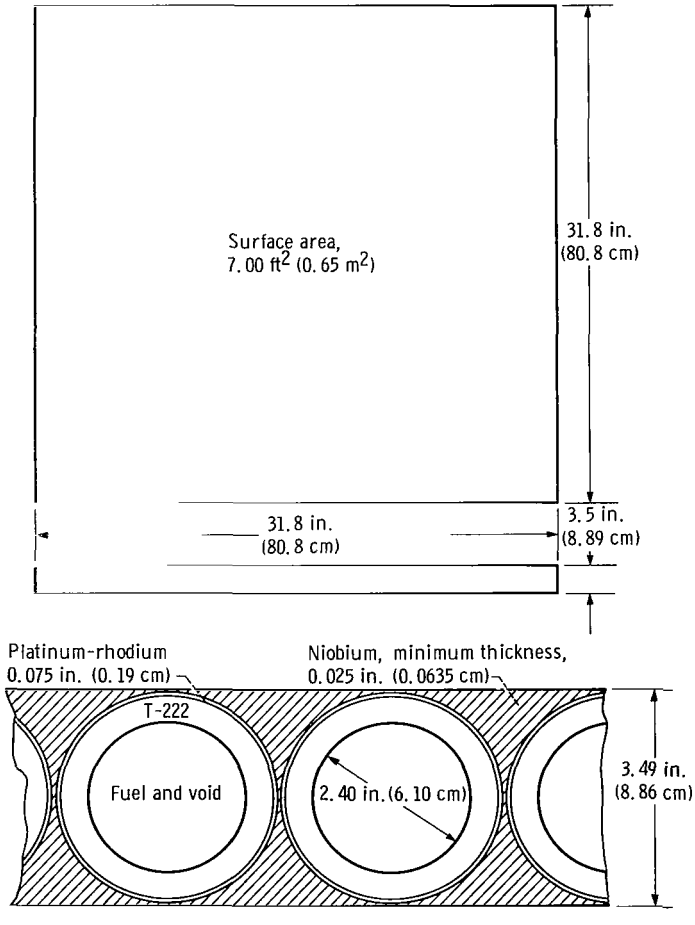


Figure 21. - Schematic diagram of fuel-block geometry.

capsules spanned the width of this block. Each capsule had an inner diameter of 2.40 inches (6.10 cm) in which the plutonium fuel would be placed. A tantalum alloy (T-222) was used as the strength-bearing member. The T-222 wall thickness (0.445 in., or 1.13 cm, in this case) was determined to withstand the maximum pressure (12 500 psi, or 86.1 $MN/m^2$) at $2460^{\circ}$ R ($1367^{\circ}$ K) from the helium generation during the isotope decay. A 0.075-inch- (0.19-cm-) thick layer of platinum-rhodium was employed to resist oxidation and Earth-substance corrosion. For the fuel block material, a high-melting-point material (over $3460^{\circ}$ R, or $1900^{\circ}$ K) with reasonable strength in the $2460^{\circ}$ R ($1367^{\circ}$ K) range was needed. This led to consideration of the refractory metals. Other desirable characteristics were relatively low density and high thermal conductivity. Niobium was selected as a compromise and because it does not form a volatile oxide. Although oxygen embrittlement will take place in the Earth's atmosphere, the block should remain intact. All radiant surfaces (niobium) of the fuel block were assumed to be coated with iron titanate for high emittance.

Additional studies of the radioisotope heat source concept are reported in reference 8. Our philosophy was that the radioisotope fuel must be contained during all credible events. In reference 8, the block concept has been replaced by an array of individual capsules supported within a bank of tubes mounted on a reentry body. Resulting heat transfer is then by radiation from the capsules to the tube holders to the heat-source heat exchanger. The individual fuel capsules are then sized so that burial on reentry will not result in a capsule meltdown and fuel release.

The present procedure assumed that all fuel-block radiant surfaces had an emittance of 0.86 and an overall coefficient of thermal conductivity for the composite block of 40 Btu per hour per foot per $^{\circ}$F or 250 kilojoules per hour per meter per $^{\circ}$K. Requirements based on capsule burial were not included in determining capsule and block size.

The weight and size trends are assumed to be representative of the general heat source philosophy, although the fuel block concept is not currently being pursued. Required surface area for thermal radiation interchange between the heat source and heat exchanger for the fuel block and the tube arrays of reference 8 were approximately the same. However, the heat source weights in reference 8 are somewhat lighter (approximately 20 percent), because of the difference in construction.

Unless noted otherwise, the fuel block reference conditions for this analysis are as follows: unaugmented ($\theta$ = 1, no fins), single-sided thermal interchange between the block and heat exchanger; one layer of fuel capsules; capsule void volumes sized for an internal pressure of 10 000 psi (69 $MN/m^2$) at approximately 130 years (ref. 2).

Figure 22 presents the variations of fuel-block surface area and weight over a range of turbine inlet temperatures for the reference conditions and explores some possible alternate limitations. For each case in this figure, the fuel block reached the maximum temperature of $2460^{\circ}$ R ($1367^{\circ}$ K). Three cases are shown with limiting "normal" heat

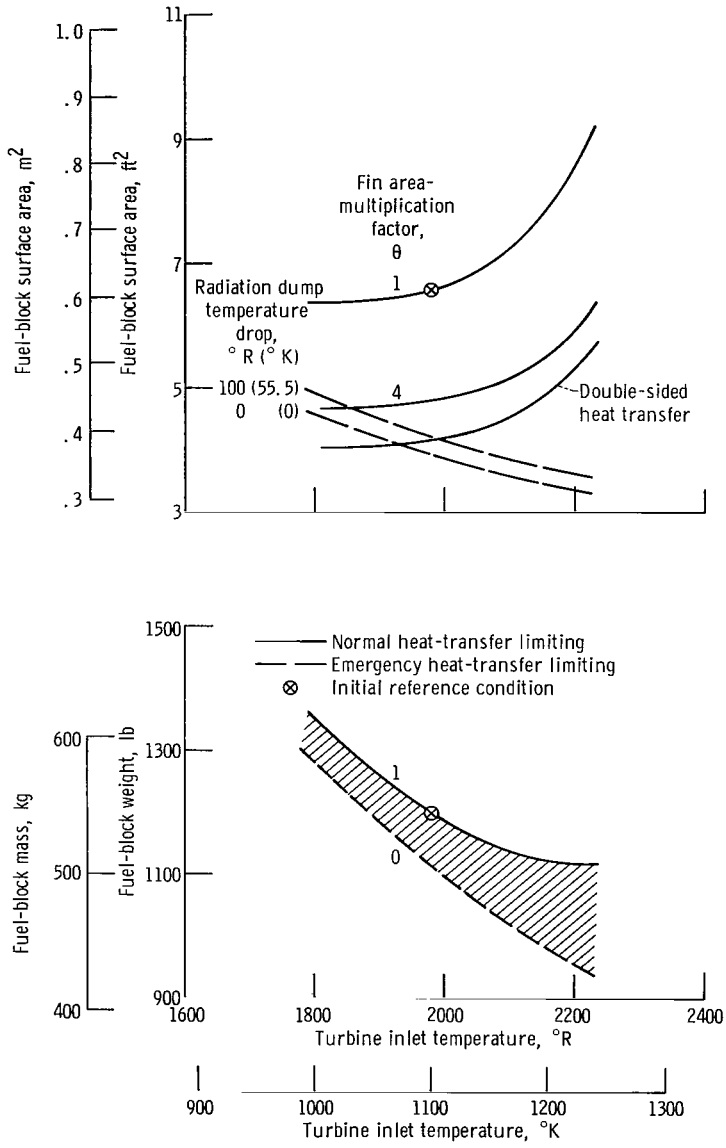


Figure 22. - Effect of turbine inlet temperature on fuel-block surface area and weight. Gross shaft power, 6.875 kilowatts; capsule internal pressure, 10 000 psi (69 MN/m$^2$). (All other initial reference conditions of table I apply.)

transfer (i.e., during radiant thermal transfer to the heat-source heat exchanger). These are for (1) the reference conditions ($\theta$ = 1), (2) single-sided heat transfer augmented by intermeshing fins on both the fuel-block and heat-exchanger surfaces ($\theta$ = 4), and (3) heat transfer from both large faces of the fuel block ("double-sided" heat transfer). A constant temperature drop of $50^{\circ}$ R ($28^{\circ}$ K) was assumed between the working gas and the heat-source heat-exchanger external surface temperature. For normal heat-transfer limiting, the temperature limit was reached near the fuel-block surface facing the reentry body (fig. 2) for single-sided heat transfer and at the fuel-block center for double-sided heat transfer. Two cases are shown with limiting "emergency" heat transfer (i.e., when the encapsulated energy must be capable of being rejected to the environment from an exposed surface). These are for (1) direct dumping from the fuel-block surface as would occur if the entire reentry body and fuel block were pivoted out of the spacecraft ($0^{\circ}$ radiation dump temperature drop), and (2) indirect dumping from an equal surface area but at a lower temperature, as might occur if the energy could be rejected through the reentry body after opening the insulated spacecraft hatch (fig. 2).

The maximum surface area and weight were required of the fuel block for the assumed reference unaugmented conditions (solid curve, $\theta$ = 1). As turbine inlet temperature is increased, cycle efficiency is increased and consequently, the thermal inventory required is decreased. However, the temperatures to which the fuel block radiates its energy also is increased and thus eventually requires an increase in surface area in order to maintain the maximum fuel-block temperature. The required surface area is relatively constant up to a turbine inlet temperature of $1900^{\circ}$ R ($1056^{\circ}$ K) and then increases while the block weight continuously decreases over the temperature range from $1800^{\circ}$ to $2200^{\circ}$ R ($1000^{\circ}$ to $1222^{\circ}$ K). The decrease in fuel-block weight was caused by the decreased fuel inventory and a thinner block, in spite of the increase in surface area.

Another limiting mode for the fuel block is the requirement of emergency heat dump directly from the fuel-block surface (dashed line, $0^{\circ}$ R, radiation dump temperature drop). This case represents the size of fuel block that can satisfy the emergency requirement, and if the normal requirements could be altered, it represents the minimum size. Because the normal temperature limitation was ignored, the surface area and weight of the fuel block continued to decrease with increasing turbine inlet temperature as a result of the decreasing radioisotope inventory. The two heat-transfer modes form a limited band of fuel-block weight. The weights shown, however, are of course dependent on the fuel-block concept which represents a conservative approach and perhaps a pessimistic weight.

Alternate arrangements for normal heat transfer might utilize either finning to enhance the radiation interchange, or radiation from both large faces of the fuel block, or both. The solid curve ($\theta$ = 4) shows the effect of finning both fuel block and heat-source heat exchanger so that the effective, single-sided, heat-transfer area is increased

by a factor of 4. The number and size of fins for this amplification has not been analyzed, nor has the mechanical complexity of the physical arrangement been determined. However, the assumption ($\theta$ = 4) reduced the single-sided, unfinned surface area requirements by about 27 percent. The effect of double-sided radiation heat transfer also reduced the fuel-block surface-area requirements for the normal-mode limitation. The unaugmented double-sided heat transfer reduced the surface area by about 36 percent from the reference case. For the emergency-mode limitation, the effect of a 100° R (or 56° K) temperature drop (such as might occur from the assumed geometry of a fuel block placed in a reentry body) before radiation to the environment, was also determined. This additional temperature drop required the fuel-block surface area to increase about 7 percent over the unrestricted emergency-mode case.

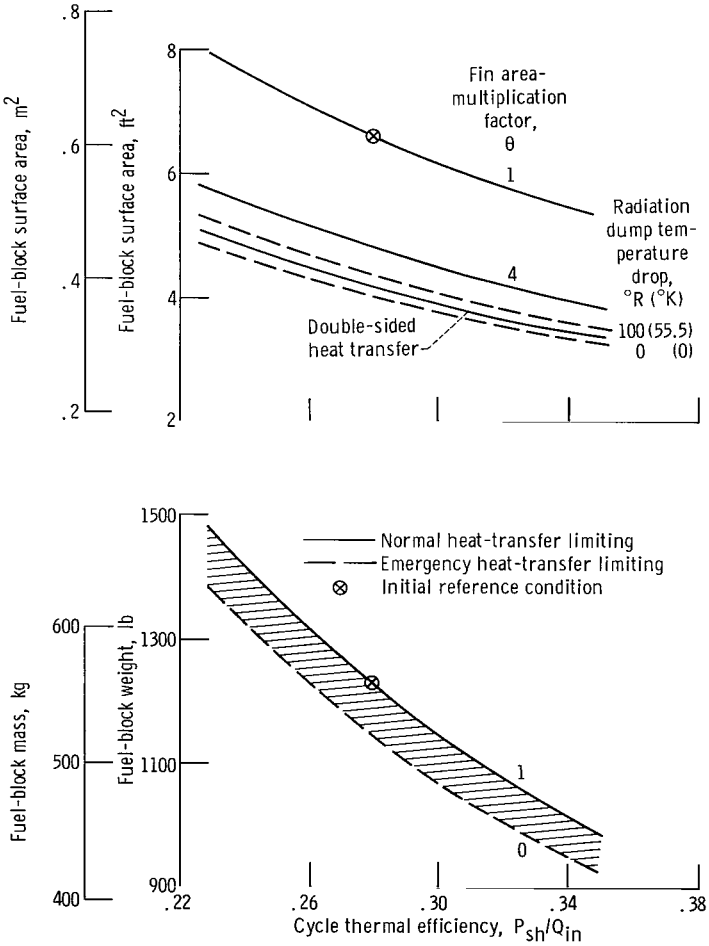


Figure 23. - Effect of cycle thermal efficiency on fuel-block surface area and weight. Gross shaft power, 6.875 kilowatts; turbine inlet temperature, 1960 °R (1089° K); capsule internal pressure, 10 000 psi (69 MN/m$^2$).

Since each mode in figure 22 ignored the temperature limitation of the other mode, a composite variation of fuel-block surface area requirements with turbine inlet temperature might be required, depending on the chosen alternatives, to avoid exceeding $2460^{\circ}$ R ($1367^{\circ}$ K) in both these modes. For example, if the ground rules were double-sided, unaugmented, normal heat transfer and emergency heat transfer with a $100^{\circ}$ R ($56^{\circ}$ K) temperature drop before radiation dumping, the variation of surface area with turbine inlet temperature would follow the dashed $100^{\circ}$ R ($56^{\circ}$ K) line up to a temperature of $1990^{\circ}$ R ($1106^{\circ}$ K), where a minimum surface area of 4.2 square feet (0.39 $m^2$) would occur, and after which would follow the solid double-sided heat-transfer line.

Although these alternatives yielded smaller surface areas and weights (which would also reflect in less shield weight), they were not pursued, and the single-sided, unaugmented, normal heat-transfer-limited blocks were used in the text. There is an advantage in utilizing a large block limited for normal heat transfer; that is, during the emergency mode, which may be the greater portion of its life if it is not recovered, the maximum fuel block temperature is considerably less than $2460^{\circ}$ R ($1367^{\circ}$ K). This, of course, would favor most material requirements for long-term containment.

Figure 23 presents the variations of fuel-block surface area and weight with cycle efficiency for the same limiting modes in the preceding figure. For each limiting mode, the variation of surface area with cycle efficiency was nearly linear. Hence, the specific area density for a fixed turbine inlet temperature and the block reference condition were constant. In all cases, increasing cycle efficiency decreased fuel-block surface area and weight. For the reference case ($\theta$ = 1, solid line), both surface area and weight decreased by about 28 percent from a cycle efficiency of 0.24 to 0.34.

Typical variations of fuel-block size and weight with design maximum internal pressure are shown in figure 24. Increasing the design maximum internal fuel capsule pressure continuously decreases the fuel capsule inner diameter for a fixed inventory. As the capsules become smaller, the overall fuel-block thickness decreases until the increased wall thickness required by the higher pressure overrides the decrease in capsule inner diameter. In figure 24, this minimum block thickness occurred at a maximum pressure of 10 000 psi (69 $MN/m^2$). Required fuel-block surface area continuously decreased over the range in design pressure from 4000 to 20 000 psi (27 to 140 $MN/m^2$), while fuel-block weight exhibited a minimum of 7500 psi (52 $MN/m^2$). Since the fuel-block surface area was still decreasing above 7500 psi (52 $MN/m^2$), the combined weight of fuel block and shield may still decrease above this pressure.

The relative weights of fuel block, shield, and their sum are shown in figure 25 as a function of the design maximum internal fuel capsule pressure. Because of the smaller fuel-block face area for a fixed inventory, the shield weight continuously decreased with increasing design pressure. Hence, the opposing effects of fuel-block weight and shield weight exhibited an insensitive minimum at about 12 000 psi (86 $MN/m^2$).

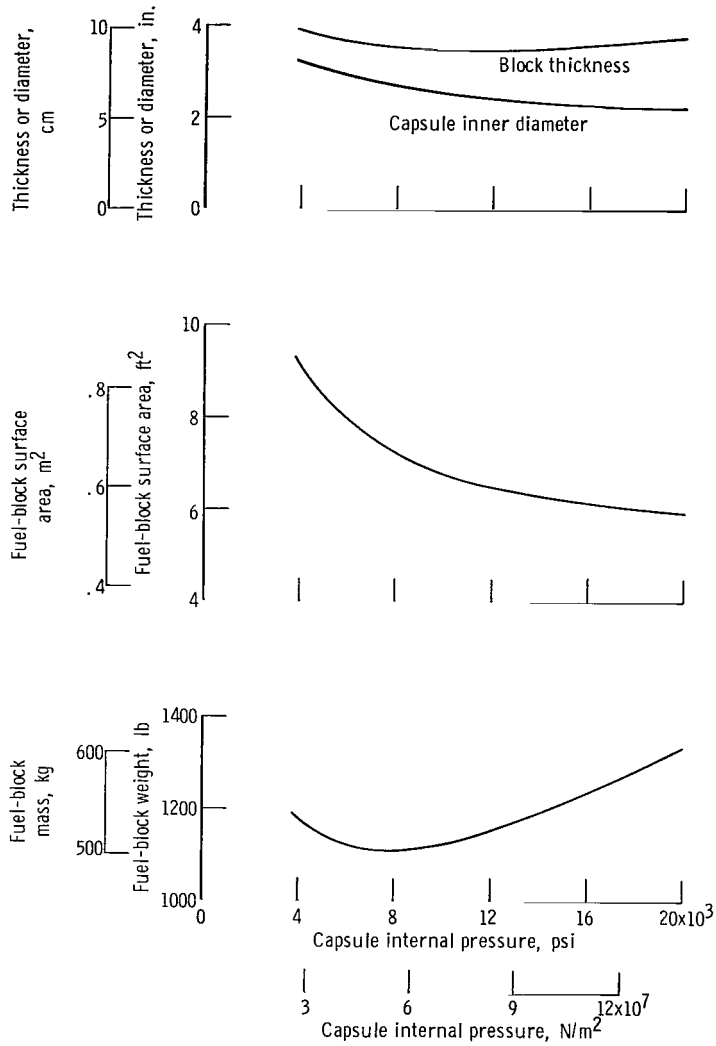


Figure 24. - Typical fuel-block variations with internal fuel capsule pressure. Gross shaft power, 6.875 kilowatts; turbine inlet temperature, 2060° R (1144° K); cycle efficiency, 0.314; fin area-multiplication factor, 1.

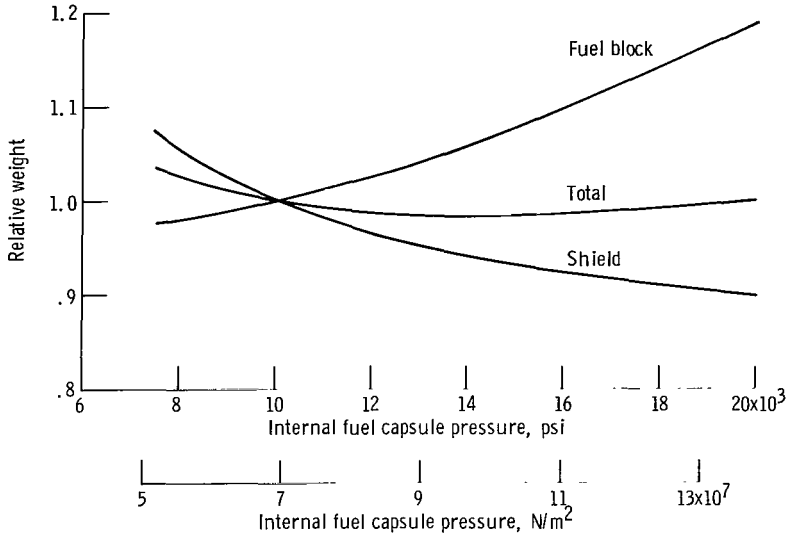


Figure 25. - Effect of design internal fuel capsule pressure on relative heat source weights. Gross shaft power, 6.875 kilowatts; dose rate at 10 feet (3 m), 5 millirems per hour.

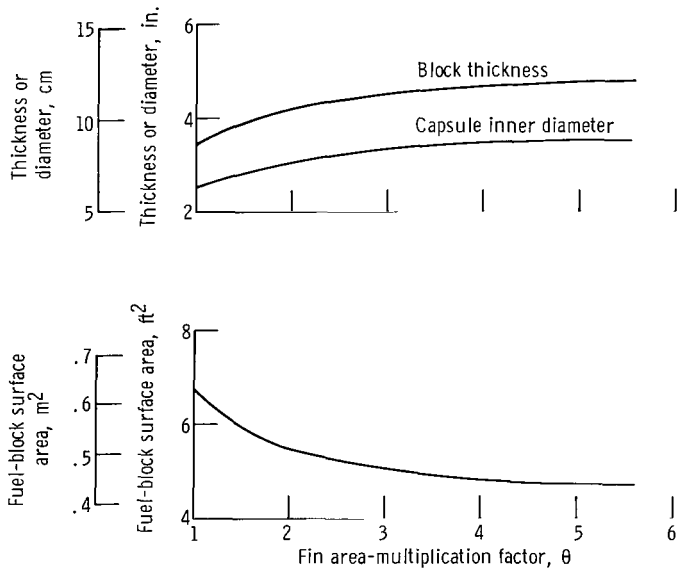


Figure 26. - Typical effects of finning on fuel-block size. Gross shaft power, 6.875 kilowatts; turbine inlet temperature, 2060° R (1144° K); cycle efficiency, 0.314.

Effects of varying the number of layers of fuel capsules were analyzed for a fixed thermal inventory. Increasing the number of layers with the capsules in a hexagonal array decreased the fuel capsule inner diameter but increased the block thickness. The increase in layers increased the number of fuel capsules, while the required surface area was essentially unchanged. Fuel-block weight, however, increased by about 12 percent from one layer of capsules to two.

Typical effects of finning on fuel-block size are shown in figure 26 for a continuous variation of the fin area-multiplication factor from 1 to almost 6. Required surface area was decreased by about 30 percent over this range, however, about 60 percent of the reduction occurred going from no fins to an area factor of 2. Hence, a relatively small amount of finning appears to go a long way in reducing the area requirements. However, both fuel-block thickness and capsule inner diameter required increases due to finning. The finned concept seems to warrant further detailed investigation.

# APPENDIX E

# HEAT-EXCHANGER ANALYSIS

by John L. Klann, Gabriel N. Kaykaty, Paul T. Kerwin, and Darl D. Bien

Brief descriptions of the calculations and typical results are presented for each of the cycle heat-transfer components. For each of these components, the calculation employed digital computer programs and assumed particular core geometries. Furthermore, a section is included on the allocation of component pressure drops.

## Heat-Source Heat Exchanger

This component was assumed to be a simple, once-through, plate-fin heat exchanger and was matched to the radiation area of the fuel block and the cycle requirements. The large surface of the heat exchanger was assumed to be square. For a given set of requirements, the product of the number of fins per foot and the fin thickness was varied over an appropriate range. At each value of this product, the fin height was determined by satisfying the heat load and an assigned pressure drop. Enough solutions were obtained to indicate both the minimum volume and minimum weight heat exchangers.

Figure 27 presents the heat-source heat-exchanger weights and volumes as a function of percent pressure drop $\Delta p/p$ and system power level. The solid lines show the constant power minimum volume heat exchangers which were used for system performance calculations. The dashed lines indicate some typical minimum weight results at constant power. As system power level was decreased, heat-exchanger heat load and pressure level also were decreased. These effects are opposing; that is, for the same pressure level, decreasing heat load would decrease weight, while for the same heat load, decreasing pressure level would increase weight. The net effect shown in figure 27 was the relatively small change in weight and volumes among the three power levels. Above about a 3-percent pressure drop, all three power levels exhibited the same rates of change of slightly decreasing weights and volumes with increased pressure drop. At lower values of pressure drop, the 2-kilowatt heat-exchanger weights became heavier than either the 6- or 10-kilowatt solutions.

For comparison, the minimum-weight solution at the 2-kilowatt power level and the volume for the 10-kilowatt-power-level minimum-weight solution are presented in figure 27. With increased pressure drop, the difference between minimum weight and volume decreases. In the range of pressure drop of interest (2 to 3 percent), for 2 kilowatts system power, the minimum-weight solution was about 30 pounds (13.6 kg) lighter than

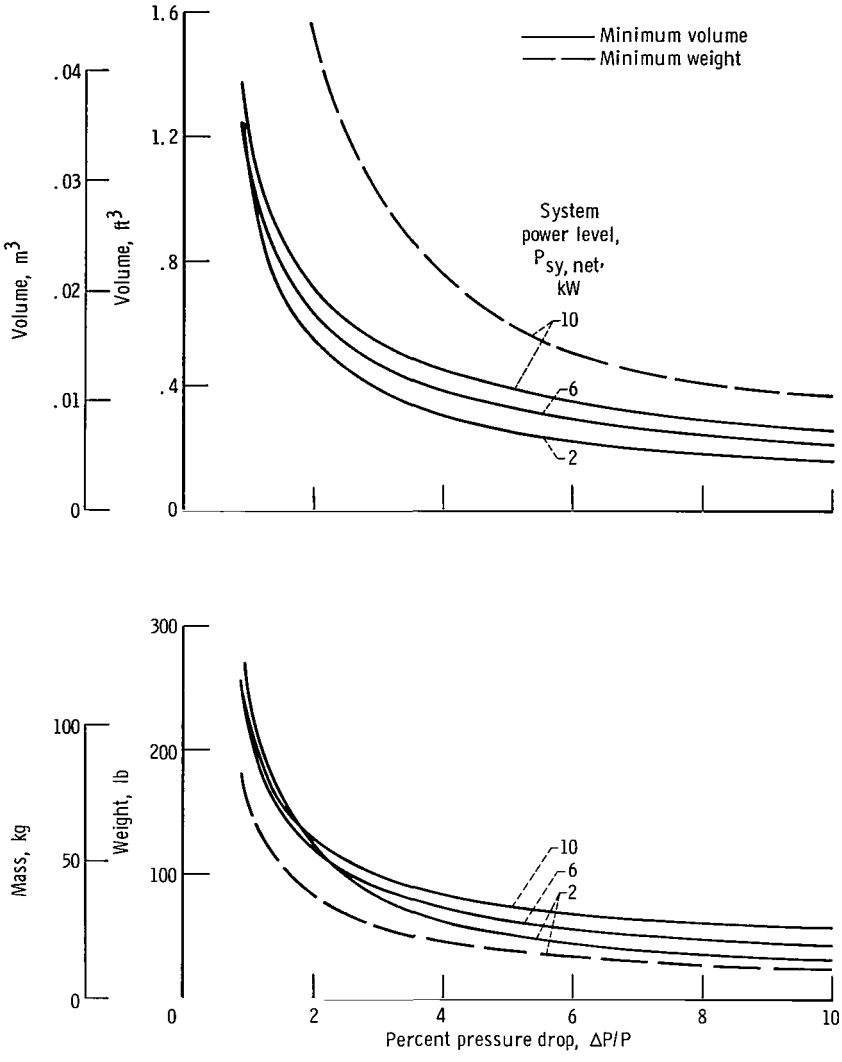


Figure 27. - Effect of pressure drop on reference system heat-source heat exchangers.

the minimum-volume solution, while at the 10-kilowatt level, the minimum-volume solution was about 0.6 cubic feet (0.017 $m^3$) smaller than the minimum-weight solution. Since this exchanger was included in the shielded volume, the relatively small increase in heat-exchanger weight probably would be justified by use of the thinnest heat exchanger.

The relative effect of working fluid and molecular weight on the heat-source heat-exchanger weight (minimum-weight solutions) was explored and is presented in figure 28. A helium-xenon mixture at a molecular weight of 83.8 is the reference, and other working fluids are compared with it. Differences among the working fluids were smallest at the 10-percent pressure drop where the use of krypton would increase the heat-exchanger

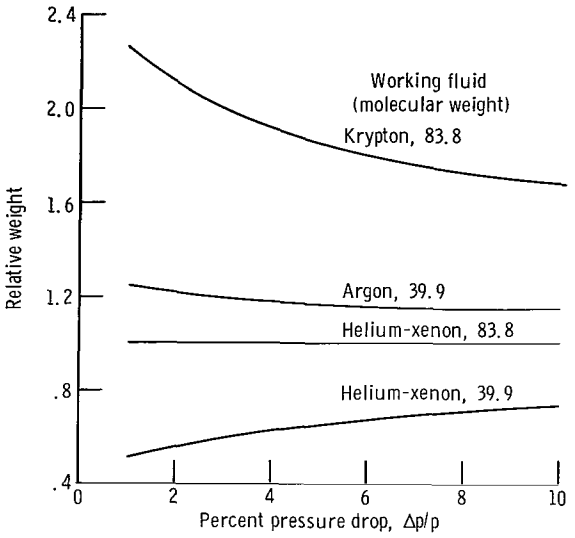


Figure 28. - Effect of working fluid on relative weight of heat-source heat exchanger (minimum-weight solutions).

weight 68 percent. However, in the range of interest (e.g., at a 3-percent pressure drop), changing from a helium-xenon mixture, at the respective molecular weight, to either argon or krypton would about double the heat-exchanger weight. A similar relative weight relation was noted for the recuperator.

## Recuperator

The recuperator in this analysis was assumed to have the same construction as the recuperator in reference 1. A rectangular, offset fin, counterflow core with triangular end sections was used. The high-pressure-side and low-pressure-side core geometries were those of figures 10-58 and 10-59, respectively, of reference 12 with the splitter plates removed. The core face area was assumed to be square. For a given set of cycle conditions, the length for a desired heat load (including effects of axial conduction) and effectiveness was calculated as a function of the face area. Pressure drops were then determined from manifold to manifold for each side including contraction, expansion, turning, and friction losses. Total recuperator percent pressure drops were used as the sum of the high- and low-pressure-side percent pressure drops.

Figure 29 presents the variations of total recuperator weight and core volume with total percent pressure drop as a function of assigned effectiveness. These are typical results and were those used in the construction of figures 13 and 14. A dashed line indicates the values of pressure drop which were assigned to the recuperator for minimum

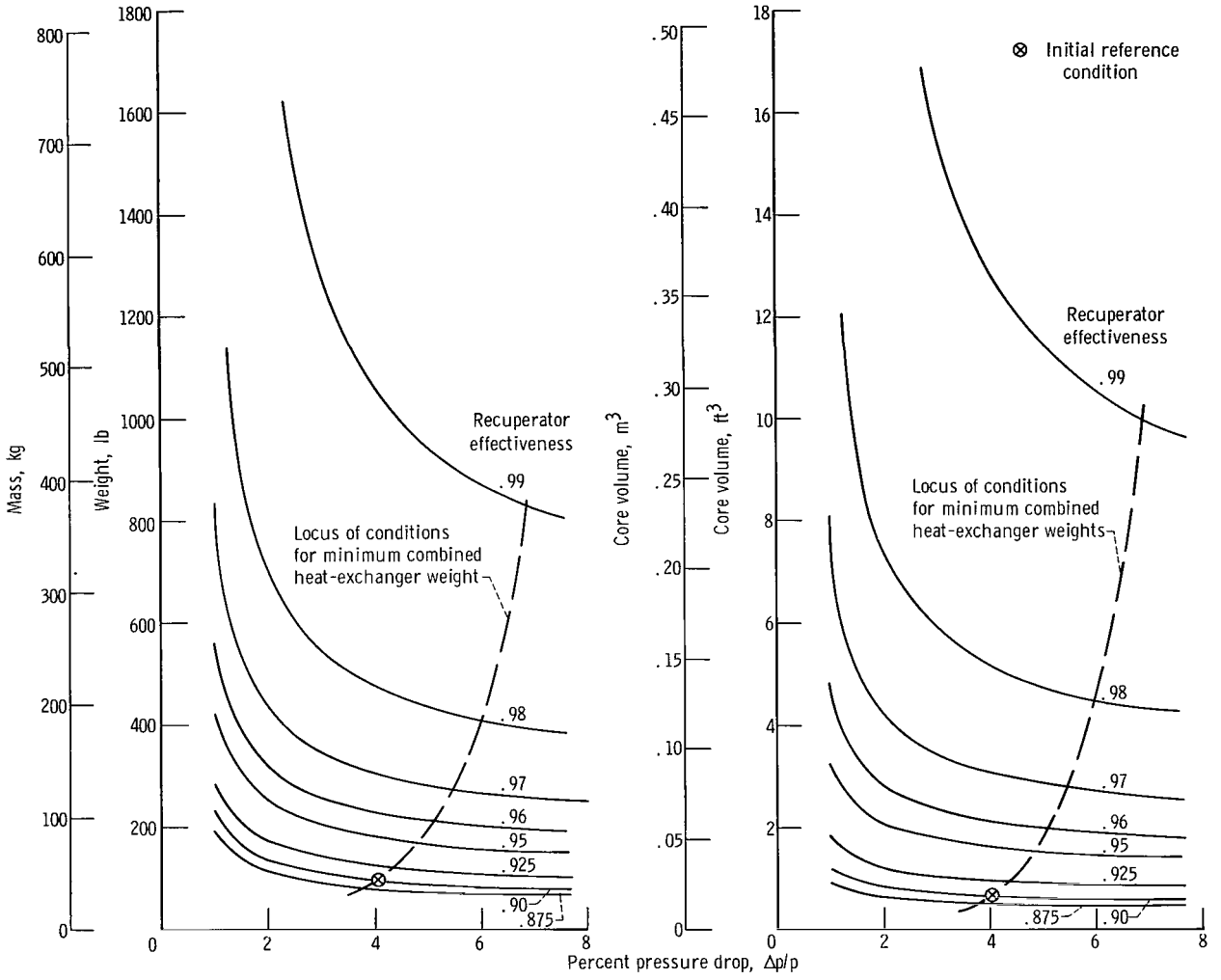


Figure 29. - Effect of pressure drop on recuperator weight and core volume. Gross shaft power, 6.875 kilowatts. (All other initial reference conditions of table I apply.)

combined heat-exchanger weight. The assigned pressure drops increased from 3.8 percent at an effectiveness of 0.875 to 6.9 percent at an effectiveness of 0.99. Both weights and volumes became large as full recuperation was approached. For values of effectiveness between 0.875 and 0.95, the changes in weight variations with pressure drop were nearly the same. However, at higher values of effectiveness, the variations in weight were a function of the level of recuperation.

## Heat-Sink Heat Exchanger

The heat-sink heat exchanger was assumed to be a multipass, cross-counterflow device with a finned tube core. The core was that of figure 10-84 in reference 12. The exchanger was sized to fit directly on the appropriate end section of the recuperator. Then, the number of passes was increased from 1 until the desired effectiveness (0.950 ±0.001) was attained. Associated core pressure drops were calculated, and as an ap-

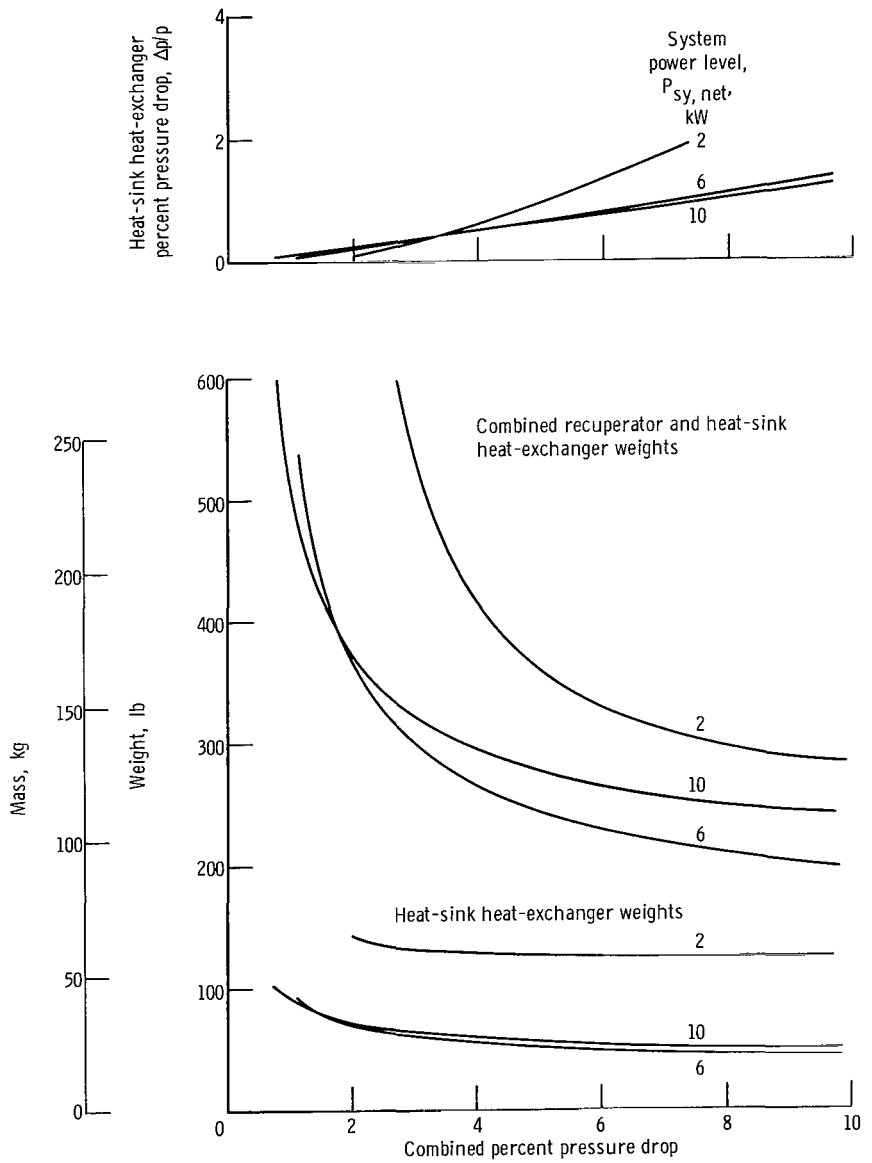


Figure 30. - Variations of reference system recuperator and heat-source heat-exchanger with combined pressure drop.

proximate allowance for manifolding, the gas-side percent pressure drop was doubled. Since the mating of the recuperator and heat-sink heat exchanger was assumed, the weights and percent pressure drops of these components were combined for the analysis.

Figure 30 presents the heat-sink heat-exchanger weights, the combined recuperator and heat-sink heat-exchanger weights, and the heat-sink heat-exchanger percent pressure drop as functions of the combined pressure drop and system power level. At 2 kilowatts, the heat-sink heat exchanger was at most 45 percent of the combined weight, whereas at 6 and 10 kilowatts the heat-sink heat exchanger was less than 23 percent of the combined weight. The reduction of power level results in the conflicting effects of reduced heat load and pressure level. The 6-kilowatt combined heat exchanger above a combined pressure drop of 2 percent exhibited the smallest weights.

## Pressure Drop Distributions

The criterion employed to determine the gas pressure drop split among the heat exchangers was that which resulted in minimum combined weight of the recuperator, heat-sink heat exchanger, and minimum-volume heat-source heat exchanger. This criterion is satisfied when the slopes of the weight against pressure drop curves for each of the three components are equal.

Figure 31 presents the pressure drop distributions used in this analysis. Percent pressure drops are shown for the recuperator, heat-source and heat-sink heat exchangers along with the system total for the investigations of the effects of recuperator effectiveness, loss pressure ratio, and system power level. The piping percent pressure drop was assumed to be 1 percent for the investigations of recuperator effectiveness and loss pressure ratio, while 1.5 percent was assumed for the final reference cases. For all cases, the recuperator needed the largest pressure drop, while the heat-sink heat exchanger needed the smallest. As recuperator effectiveness was increased, the pressure drop allocated to it also increased with the necessity of decreasing allocations to the remaining components. For increasing loss pressure ratio, all distributions decreased linearly. For a total system loss pressure ratio at the 0.92 level from 2 to 10 kilowatts, the recuperator and heat-sink heat exchanger percent pressure drops decreased, while the heat-source heat exchanger percent pressure drop increased.

## Radiator

A cylindrical, unoriented radiator with longitudinal tubes and circumferential headers on a 260-inch- (6.6-meter-) diameter vehicle was assumed. Two tubes (one redundant)

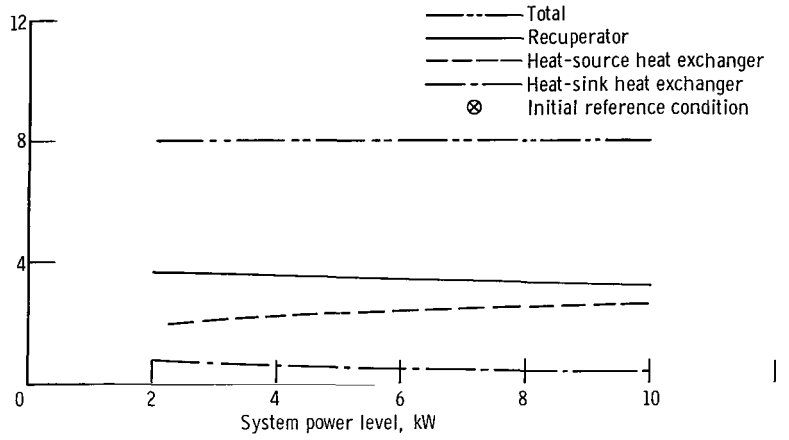


(a) Effect of system power level.

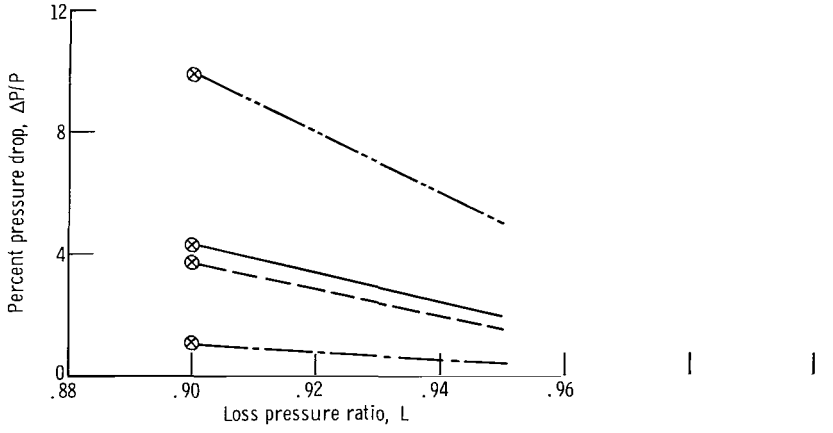


(b) Effect of loss pressure ratio.

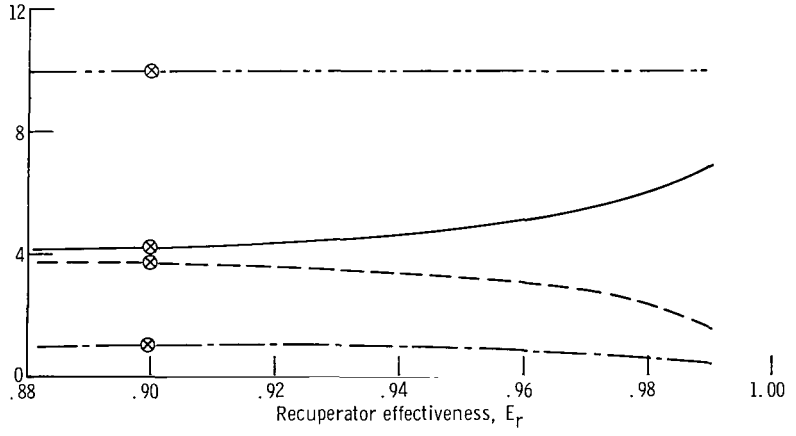


(c) Effect of loss pressure ratio and recuperator effectiveness. Gross shaft power, 6.875 kilowatts.

Figure 31. - Heat-exchanger pressure drop distributions for minimum combined weight.

were assumed for each fin, and calculations were made for a probability of success of 0.995 against meteoroid penetration for a 5-year mission. FC-75 (a fluorochemical) was assumed to be typical of the class of coolants suitable for this application, and its heat-transfer properties were used in the calculations. The computer program of reference 18, modified for cylindrical geometry, was employed. Whipple's 1963A meteoroid flux model was assumed along with a meteoroid density of 0.2 gram per cubic centimeter and an average velocity of 65 000 feet per second (19 800 m/sec). Heat rejection was assumed to occur only from the outside cylindrical surface, and the inside surface armor was reduced because of the bumper effect by the method of reference 19. Liners inside the tubing were assumed with a resulting spall factor of 1.4.

Typical results for the radiators are shown in figure 32. The effects of system power level on radiator area and weight are shown. The curves shown are the loci of minimum radiator weights as a function of surface area; that is, the number of tubes on the fixed diameter was varied until the combined effectiveness of tubes and fins resulted in a minimum weight. For each power level, the minimum value of required radiator area appears to approach a value of 65 square feet per kilowatt (6.04 $m^2$/kW) of system

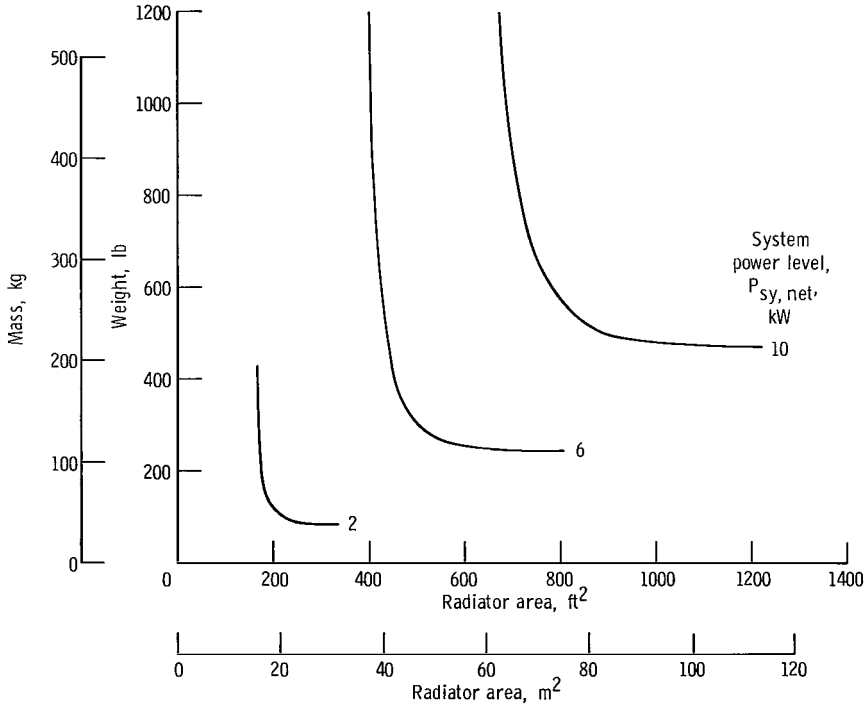


Figure 32. - Effect of power level on reference system radiator area and weight.

output. Minimum radiator weights, on the other hand, were reached at a value of about 125 square feet per kilowatt electric output (11.6 $m^2$/kWe).

In those parts of the analysis where fixed radiator areas were assumed, radiator weight variations are the result of reoptimization of the number of tubes and fin thickness for the changes in radiator conditions with the parameter in question.

# APPENDIX F

## SYSTEM EFFICIENCY CALCULATIONS

Overall system efficiency used in this analysis was defined as

$$\eta_{sy} \equiv \frac{P_{a,net}}{Q_{in,g}} \tag{F1}$$

where

$$Q_{in,g} = 1.048\ (Q_{in} + L_i) \tag{F2}$$

$$P_{a,net} = P_a - P_k - P_p \tag{F3}$$

The raw alternator terminal power was defined as

$$P_a \equiv \eta_{a,em} P_{sh,net} \tag{F4}$$

where

$$P_{sh,net} = P_{sh} - L_w - L_s - L_j - L_t \tag{F5}$$

where

$$P_{sh} = \eta_{cy} Q_{in} \tag{F6}$$

Hence,

$$\eta_{sy} = \frac{\eta_{a,em}(P_{sh} - L_w - L_s - L_j - L_t) - P_k - P_p}{1.048\ (Q_{in} + L_i)} \tag{F7}$$

Allowances were made for heat-source thermal loss $L_i$, system control power $P_k$, and radiator pump power $P_p$, while estimates were made for alternator electromagnetic efficiency $\eta_{a,em}$, windage loss $L_w$, shaft seal loss $L_s$, and bearing friction losses $L_j$ and $L_t$.

Gross shaft power $P_{sh}$ was assumed to be directly proportional to cycle mass flow rate. Corrections of turbine and compressor efficiency due to variations in Reynolds number (eq. (B7)) were small and hence were neglected. The required cycle thermal input $Q_{in}$ for a fixed gross shaft power was determined from the calculated cycle efficiency (eq. (F6)). The heat-source insulation loss $L_i$ at the end of the 5-year mission was assumed to be 5 percent of the cycle thermal input. The gross initial heat-source energy $Q_{in,g}$ then followed from equation (F2) where the factor 1.048 allowed for plutonium 238 decay over the 5-year mission and an assumed 90-day launch delay.

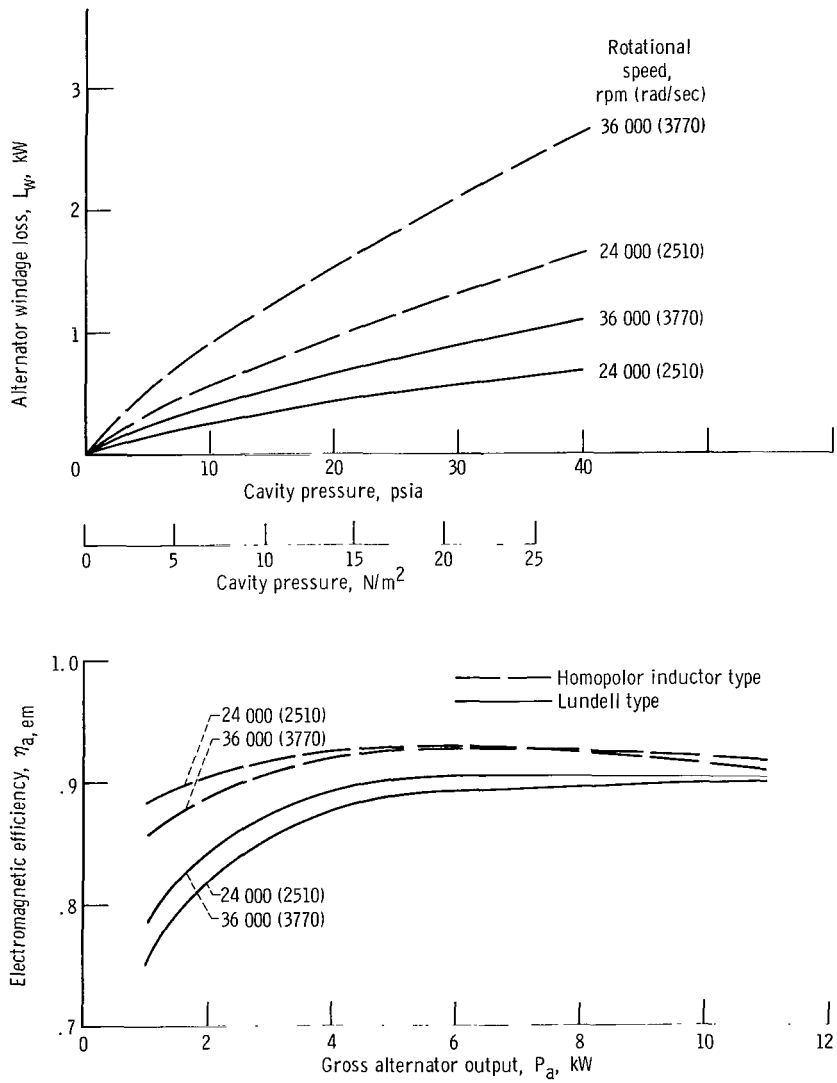


Figure 33. - Effect of alternator type, power level, and cavity pressure on efficiency and windage losses.

Results of an unpublished alternator sizing study which were employed in the calculations of this analysis are shown in figure 33. Alternator windage loss as a function of cavity pressure and electromagnetic efficiency as a function of gross alternator power output are presented for two rotational speeds and two alternator types. Alternator and bearing cavity pressures were assumed to be 75 percent of the compressor discharge pressure. For rotational speeds of 24 000 and 36 000 rpm (2510 and 3770 rad/sec), the rotor diameters for either type of alternator were conservatively estimated as 4.2 and 3.6 inches (10.7 and 9.14 cm), respectively. Although the Lundell-type alternator had lower electromagnetic efficiencies than the homopolar-inductor type, its windage losses were considerably smaller than those of the homopolar-inductor type. On the basis of overall performance, the Lundell-type alternator was preferred and the 36 000-rpm (3770-rad/sec) characteristics were used in the analysis.

The alternator windage loss $L_w$ from figure 33 was used as one of the terms in equation (F5) to correct the gross shaft power to the net value available to the alternator. Other shaft windage losses were assumed to be included in the turbine and compressor efficiencies. The seal leakage loss $L_s$ assumed that 1 percent of the compressor flow was lost to the turbine to perform useful work.

Journal bearing analysis was based on the three-tilting-pad theory of reference 20, while the thrust bearing analysis employed the spiral-groove theory of reference 21.

The journal bearing loads were assumed to consist of the rotor weight and an arbitrary constant load of 3.3 pounds or 14.7 newtons (an attempt to account for other unbalanced forces). The rotor weight was scaled from the results of reference 3 by assuming a fixed weight of 8.3 pounds (37 N) and varying the remaining weight of 6.2 pounds (27.6 N) by the square of the compressor tip diameter divided by 3.0 inches or 7.6 centimeters (the compressor tip diameter of ref. 3). The total journal bearing load was then assumed to be equally split between two sets of bearings. The shaft radius was determined from the 2-kilowatt system bearing cavity pressure so that either a maximum bearing unit loading of 4 psi (27.6 $kN/m^2$) or a maximum total bearing load coefficient of 1.0 was attained. Then, the bearing design curves of reference 20 for a shoe arc length of $94.5^o$, a ratio of shaft radius to shoe length of 0.606, and a dimensionless pivot location of 0.667 were employed. A preload factor of 0.6 and a built-in shoe clearance to shaft radius ratio of 0.001 were assumed. The pad friction factor was nearly constant over a wide range of shoe eccentricity ratio; hence, the frictional forces (calculated by eq. 57 of ref. 20) and losses were assumed constant and independent of both load and pressure level.

The calculated thrust bearing losses assumed that, at a gross shaft power of 6.875 kilowatts, a net thrust load of 10 pounds (44.5 N) could be attained. This arbitrary load was varied directly with gross shaft power. The inner shaft radius was assumed to be the same as the shaft radius at the journal bearing locations. For the thrust bearing, an

inner- to outer-radius ratio 0.5 and a ratio of bearing clearance to outer radius of 0.001 was assumed. A double-acting bearing was used with a total bearing gap of 0.007 inch (0.0178 cm). Equations (D1), (D2), and (D4) of reference 21 were used to calculate both the loaded and unloaded bearing face clearances and friction losses.

The final system penalties were allowances for control power requirements and radiator pump power. Control power was assumed to be 4 percent of the alternator output, while pump power was assumed to be about 10 watts per kilowatt of thermal energy to be rejected. Subtraction of these two losses from the gross alternator output yielded the net alternator power.

## REFERENCES


1. Bernatowicz, Daniel T.: NASA Solar Brayton Cycle Studies. Paper presented at the Symposium on Solar Dynamics Systems, Solar and Mechanics Working Groups of the Interagency Advanced Power Group, Washington, D.C., Sept. 24-25, 1963.

2. Ad Hoc Study Group: Selection of Radioisotopes for Space Power Systems. NASA TM X-1212, 1966.

3. McKhann, G. G.: Preliminary Design of a Pu-238 Isotope Brayton Cycle Power System for MORL. Vol. I: Technical Summary. Rep. No. SM-48832 (NASA CR-68809), Douglas Aircraft Co., Inc., Sept. 1965.

4. Mason, John L.: Working Gas Selection for the Closed Brayton Cycle. Paper presented at the Sixth Agard Combustion and Propulsion Colloquium, Cannes, France, Mar. 16-20, 1964.

5. Senoo, Yasutoshi: Gas-Medium Selection and Turbomachinery Matching for Closed-Brayton-Cycle Space Power System. Paper No. 63-WA-86, ASME, Nov. 1963.

6. Stewart, Warner L.; Anderson, William J.; Bernatowicz, Daniel T.; Guentert, Donald C.; Packe, Donald R.; and Rohlik, Harold E.: Brayton Cycle Technology. Space Power Systems Advanced Technology Conference. NASA SP-131, 1966, pp. 95-145.

7. Wood, Homer J.: Current Technology of Radial-Inflow Turbines for Compressible Fluids. J. Eng. Power, vol. 85, no. 1, Jan. 1963, pp. 72-83.

8. Geiringer, Paul L.: Handbook of Heat Transfer Media. Reinhold Publishing Corp., 1962.

9. Robinson, R. A.; et al: Brayton-Cycle Radioisotope Heat Source Design Study. Phase I (Conceptual Design) Report. Rep. No. ORNL-TM-1691 (NASA CR-72090), Oak Ridge National Lab., Dec. 1966.

10. Robinson, R. A.; Chapman, T. G.; Ewing, S. T.; Miller, A. J.; and Nichols, J. P.: Brayton-Cycle Radioisotope Heat-Source Design Study. Phase II (Preliminary Design) Report. Rep. No. ORNL-TM-1829 (NASA CR-72151), Oak Ridge National Lab., Aug. 1967.

11. Glassman, Arthur J.: Thermodynamic and Turbomachinery Concepts for Radio-isotope and Reactor Brayton-Cycle Space Power Systems. NASA TN D-2968, 1965.

12. Kays, W. M.; and London, A. L.: Compact Heat Exchangers. Second ed., McGraw-Hill Book Co., Inc., 1964.

13. Balje, O. E.: A Study on Design Criteria and Matching of Turbomachines: Part A - Similarity Relations and Design Criteria of Turbines. J. Eng. Power, vol. 84, no. 1, Jan. 1962, pp. 83-102.

14. Balje, O. E.: A Study on Design Criteria and Matching of Turbomachines: Part B - Compressor and Pump Performance and Matching of Turbocomponents. J. Eng. Power, vol. 84, no. 1, Jan. 1962, pp. 103-114.

15. Shepherd, D. G.: Principles of Turbomachinery. The Macmillan Co., 1956.

16. Kofskey, Milton G.; and Glassman, Arthur J.: Turbomachinery Characteristics of Brayton Cycle Space-Power-Generation Systems. Paper presented at the 9th ASME Annual Gas Turbine Conference and Products Show, Houston, Mar. 1-5, 1964.

17. Balje, O. E.: A Contribution to the Problem of Designing Radial Turbomachines. Trans. ASME, vol. 74, no. 4, May 1952, pp. 451-472.

18. Saule, Arthur V.; Krebs, Richard P.; and Auer, Bruce M.: Design Analysis and General Characteristics of Flat-Plate Central-Fin-Tube Sensible-Heat Space Radiators. NASA TN D-2839, 1965.

19. Larson, J. W.: Research on Spacecraft and Powerplant Integration Problems. Rep. No. 64SD892 (NASA CR-54159), General Electric Co., July, 1964.

20. Gunter, Edgar J., Jr.; Hinkle, James G.; and Fuller, Dudley D.: Design Guide for Gas-Lubricated Tilting-Pad Journal and Thrust Bearings with Special Reference to High-Speed Rotors. Rep. No. NY02512-1, Franklin Institute Research Lab., Nov. 1964.

21. Ellis, J. N.; and Collins, F. A.: Brushless Rotating Electrical Generators for Space Auxiliary Power Systems. Lear Siegler, Inc. (NASA CR-54320, Vols. 1-5), Apr. 1965.



NASA-Langley, 1968 —— 3 E-4145

NATIONAL AERONAUTICS AND SPACE ADMINISTRATION
WASHINGTON, D. C. 20546

OFFICIAL BUSINESS

FIRST CLASS MAIL

POSTAGE AND FEES PAID
NATIONAL AERONAUTICS AND
SPACE ADMINISTRATION

POSTMASTER: If Undeliverable (Section 158 Postal Manual) Do Not Return

*"The aeronautical and space activities of the United States shall be conducted so as to contribute . . . to the expansion of human knowledge of phenomena in the atmosphere and space. The Administration shall provide for the widest practicable and appropriate dissemination of information concerning its activities and the results thereof."*

—NATIONAL AERONAUTICS AND SPACE ACT OF 1958

# NASA SCIENTIFIC AND TECHNICAL PUBLICATIONS

TECHNICAL REPORTS: Scientific and technical information considered important, complete, and a lasting contribution to existing knowledge.

TECHNICAL NOTES: Information less broad in scope but nevertheless of importance as a contribution to existing knowledge.

TECHNICAL MEMORANDUMS: Information receiving limited distribution because of preliminary data, security classification, or other reasons.

CONTRACTOR REPORTS: Scientific and technical information generated under a NASA contract or grant and considered an important contribution to existing knowledge.

TECHNICAL TRANSLATIONS: Information published in a foreign language considered to merit NASA distribution in English.

SPECIAL PUBLICATIONS: Information derived from or of value to NASA activities. Publications include conference proceedings, monographs, data compilations, handbooks, sourcebooks, and special bibliographies.

TECHNOLOGY UTILIZATION PUBLICATIONS: Information on technology used by NASA that may be of particular interest in commercial and other non-aerospace applications. Publications include Tech Briefs, Technology Utilization Reports and Notes, and Technology Surveys.

*Details on the availability of these publications may be obtained from:*

**SCIENTIFIC AND TECHNICAL INFORMATION DIVISION**

**NATIONAL AERONAUTICS AND SPACE ADMINISTRATION**

**Washington, D.C. 20546**